MODELING OF NONPLANAR PHOTOVOLTAIC ARRAYS

A Thesis

by

LANCE GABRIEL ALPUERTO

Submitted to the Office of Graduate and Professional Studies of
Texas A&M University
in partial fulfillment of the requirements for the degree of

MASTER OF SCIENCE

Chair of Committee,	Robert Balog
Committee Members,	Karen Butler-Purry
	Laszlo Kish
	Charles Culp
Head of Department,	Miroslav M. Begovic

December 2016

Major Subject: Electrical Engineering

ABSTRACT

With the recent advancements of photovoltaic (PV) material, the previous limits of solar applications have been surpassed. These developing technologies allow for implementation on nonplanar surfaces. The implications of this advancement is the ability to harvest the abundance of solar energy in facets that were previously not possible, constrained by the rigidity of traditional crystalline silicon. Conventional modeling takes advantage of the homogenous nature of flat surface view factors for accurate clear sky harvest prediction. The issue arises when this homogeneity is no longer the case like a nonplanar surface, producing a gradient of view factors. These varying view factors also create new requirements for integration with power electronics responsible for converting raw PV current into usable energy and maximum harvest. Non-homogenous view factors create unique current densities on a per cell basis such that no longer allows the interconnection requirements of an array to be arbitrarily satisfied. This thesis takes a differential approach to modeling gradients of view factors and associated generated current densities on a nonplanar surface with the intention to geometrically optimize the surface cells to maximize harvest potential as well as create a means to determine the best cell interconnections for integration with current power electronic technologies. This work shows over 45% more energy collected in some geometries when compared to a flat plate. Also, a method for minimizing the current variability of cells to be connected in series was conducted. Using K-means clustering, each cell current is analyzed and grouped, resulting in appropriate results minimizing mismatch almost completely in some arrays.

ACKNOWLEDGEMENTS

This publication was made possible by NPRP grant # 7-299-2-124 from the Qatar National Research Fund (a member of Qatar Foundation). The statements made herein are solely the responsibility of the authors.

I would first like to thank my advisor and committee chair, Dr. Balog, for the wisdom and guidance he has shared with me throughout my time with him in the Renewable Energy and Advance Power Electronics Lab. I greatly appreciate the support and knowledge you have passed on to me.

A special thank you goes out to Dr. Butler-Purry for believing in me and giving me the opportunity to work with her on a project when I first arrived to College Station. I do not know how I would have made it this far otherwise.

Thanks also go out to my committee members, Dr. Kish and Dr. Culp, for being a part of my graduate experience. You took time out to support me and my research for which I hold in high regard.

Next, I would like to thank all my friends and colleagues in the REAPER Lab. They were always there when I was in need and for that I am forever grateful. I only hope I can repay that kindness

Finally, I need to thank my parents for believing in me and, most importantly, teaching me that determination and a good attitude go a long way.

TABLE OF CONTENTS

Page

LIST OF FIGURES

Page

LIST OF TABLES

Page

CHAPTER I

INTRODUCTION

Motivation

Solar energy is one of the fastest growing renewable resources from 1990 to 2015 at an annual growth rate of about 44.1%, reaching the maximum of 174.5 TWh[1]; a fraction in comparison to the roughly approximated 89,000 TW theoretically striking the earth at any moment. From an availability standpoint, solar is the best option for renewable energy harvesting. In addition to a high potential the recent advancements in the material of photovoltaics has been showing tremendous promise regarding efficiency. Efficiency and structural limits are being pushed farther than previously thought possible.

From figure 1, by NREL, we see this trend of increasing efficiency of all types of photovoltaic materials. In addition, the price of the materials is showing a downward trend as well thanks to added research on the balance of systems costs, regarding ancillary necessities like inverters or soft costs like acquisition. It is predicted that the more solar is implemented in the US the cheaper the technology will be, trending similarly to Moore's Law of semiconductors. This trend has been seen in that of Germany where the cost per watt is 50% cheaper than that of the US[2].

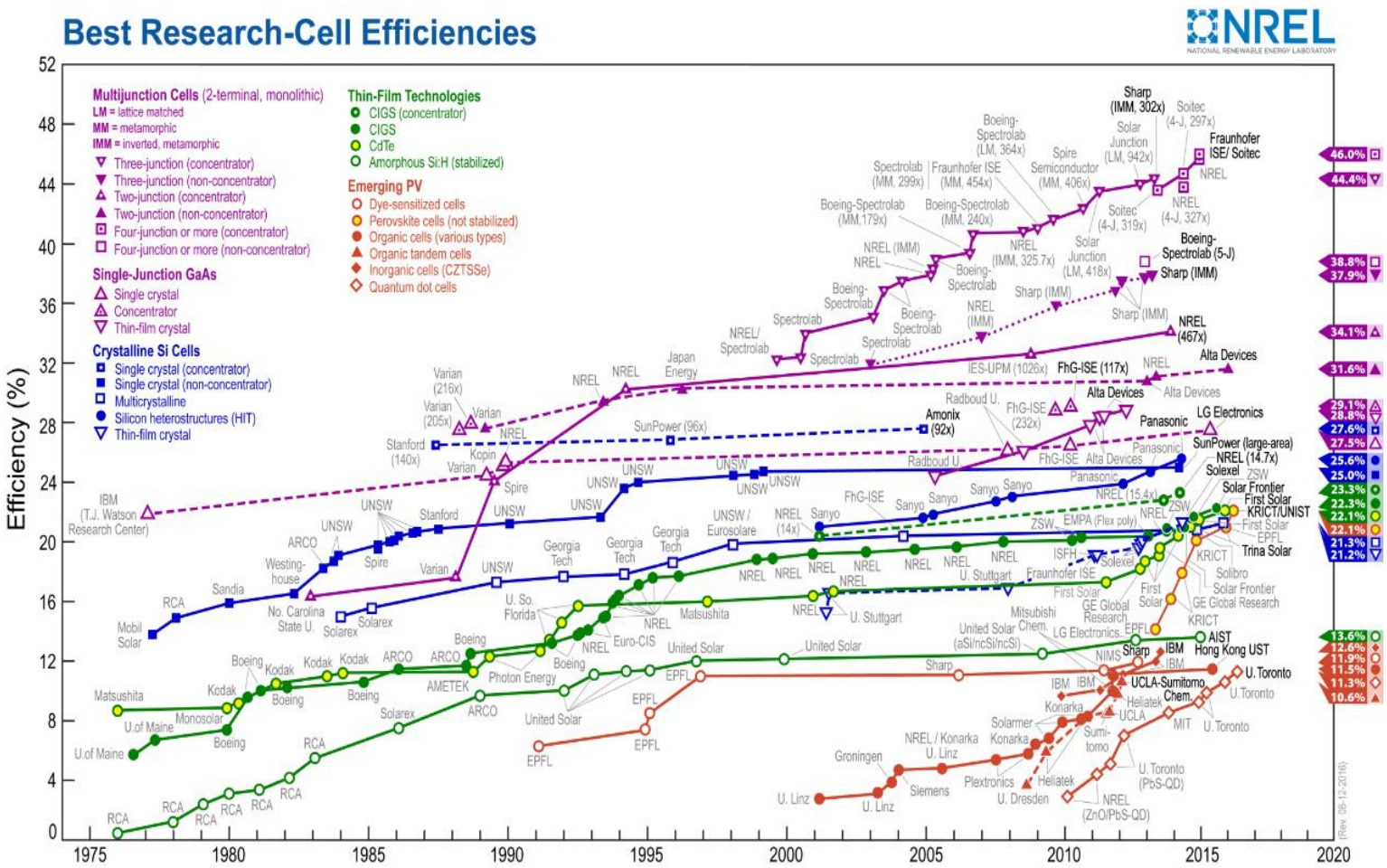

Figure 1: Best researched PV cell efficiencies by year [3]

This decline in cost of material is partly due to the development of the 3rd generation photovoltaic materials. The first being the conventional crystalline silicon solar panels. The second generation are made from layers of semiconductor material allowing for much thinner and flexible characteristics[4]. Less materials are necessary to manufacture thus costs go down, but at the expense of the efficiency of conversion. The most popular types of cells in the second generation are amorphous silicon(a-Si), cadmium telluride(CdTe), and copper indium gallium diselenide(CIGS). Even with a-Si's commercial presence there is still research going in to optimize this materials substrate interactions for increased efficiencies[5]. These three materials comprise the top three power yields commercially found[4]. The third generation is still in development in an attempt to take the best of both previous generations. Thin-film multi-crystalline silicon offer promise for efficient low cost solar cells but harnessing the absorption in the indirect bandgap is a major issue[6]. Microcrystalline silicon, gallium arsenic, dye-sensitized, and organic solar cells are just some of the more popular materials being research [4, 6].

Conventional solar cells are structurally restricted to a flat rigid plate due to the rigid makeup of the silicon photovoltaic wafer material. These thin film photovoltaic materials allow for nonplanar implementation in facets never before deemed possible. It has been confirmed that advances in thin film enables PV cells to be manufactured on flexible substrates[7-9]. Even more advances like fabricating layers of solar material on a roll-to-roll basis now allow for even further practicality of using thin film in various applications[10]. Conforming PV material onto the wings of drones[11] would supply auxiliary power for longer flights in emergency situations or military surveillance is now

possible. Another application would be personal generation using a photovoltaic material to be manufactured into fabrics [12].

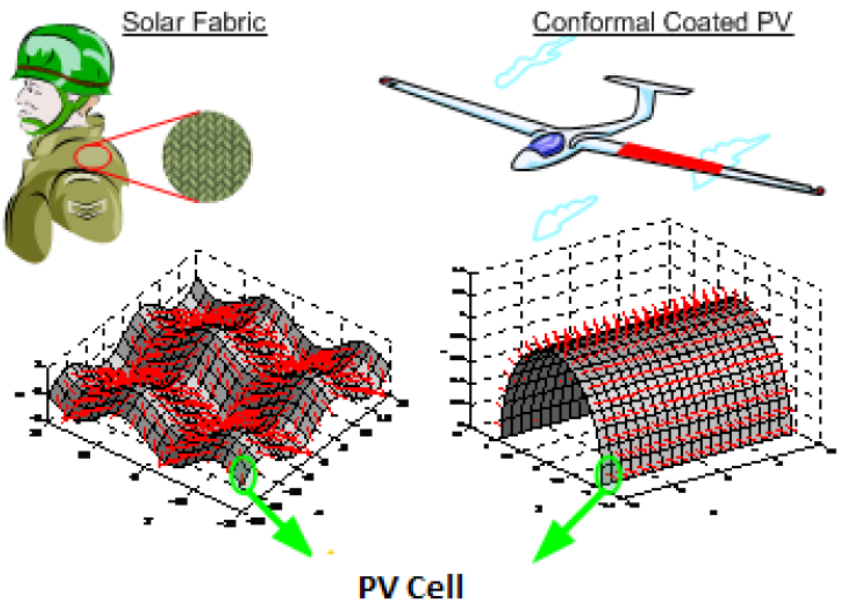

Figure 2: Practical implementation possibilities for flexible thin-film

With this expansion of practical applications there has also been investigation into the long-term performance and stability of these thin-films. In [13] they produced performance data over 30-60 months based on various US manufacturers to determine how certain materials react to hot and humid climates. Studies are also being done to better design the PV laminates [14] by way of finite element analysis which increase the stability despite the ever-changing outdoor environment.

Widespread research interest in PV results in total solar harvest increasing rapidly every year around the globe seen in figure 3; it stands to reason that there will be increasing

interest in advancing the application of solar in non-traditional fashions. This desire to use solar in a wider range of applications is the push needed to make flexible thin-film a commercial resource.

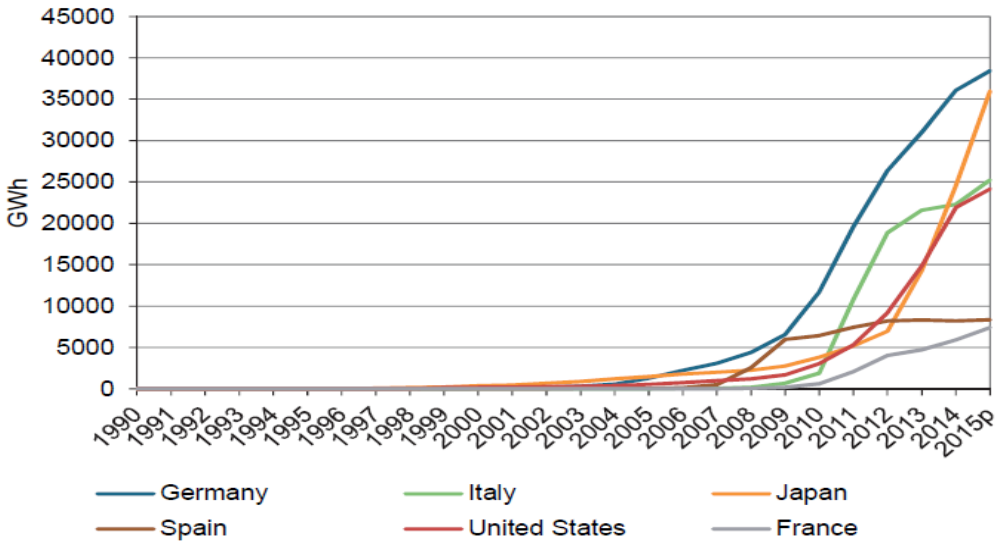

Figure 3: Solar power generation growth of select countries [1]

Significance

With increasing advancements and reductions in cost per watt there is now room to develop practical systems for these new technologies like thin film. The complexities introduced must be dealt with in order for these practical applications.

The significance would be the analysis of the gradient of incident radiation over the full surface. Irradiation seen by the solar collector is vital to the harvest of PV systems

and because of this there are many methods of calculating the energy reaching the earth. In [15] a 3D solar radiation model integrated with 3D geographical information systems facilitates the assessment of photovoltaic harvests. In [16] a predictive numerical model was developed to approximate radiation taking into account terrain surface conditions. Even more specific studies are being done to verify or approximate diffuse radiation using derivations of the direct beam radiation[17] or the H- and non-H methods[18]. This work allows radiation forecasting to be possible, but without proper modeling the PV system will most likely underperform.

Despite not having appropriate modeling for irregular surfaces, there has been a growing interest in building integrated photovoltaics (BIPV) in recent years. BIPV has many advantages over the conventional implementations. One reason being in BIPV systems the solar cells are a part of the building rather than being a standalone set up, requiring less materials and cost. An example if this would be replacing regular roof tiles with a photovoltaic cell so that it serves the same purpose but with the added benefit of harvesting energy at only 2%-5% of additional construction cost, referencing a commercial building[19]. The lack of modeling on BIPV systems is evident for two main reasons: partial shading of the array and the diversity of the incident light due to varying tilt angles of the cells[20]. The varying of tilt angles is synonymous with the idea of incident radiation gradient where cells are directed in different directions. The curve of a surface will also create this concept of varying angles that needs to be accounted for. With characterization of the curvature an analysis can be made to validate the harvest in any application desired.

Modeling of the surface to correctly account for the gradient of incident radiation is a required aspect of a PV analysis, and with this comes a gradient of current densities generated as well, further complicating the model parameters. Current density mismatch is a major issue even within planar systems of homogeneous cell orientations caused by partial shading. For nonplanar PV this mismatch is not only dictated by passing clouds but by the nature of the curved surface as well. The variability of electrical production has been researched for designing smart microgrids being run by nonplanar photovoltaics[21]. Design considerations for remote nonplanar photovoltaic systems[22] have been investigated previously also, but for optimal production to be possible research is still needed in surface modeling and current variation to make nonplanar photovoltaics a reality. A unique process to mitigate this mismatch of current density must be realized to validate practical implementations of nonplanar thin-film systems.

Individual cell geometry on a nonplanar surface is analyzed to further emphasizes the importance of understanding the characteristics of the surface. The unique characteristic of flexibility, though it may have added complexities, grants a higher potential harvest in that it can have more area to collect radiation within the same footprint as a flat plate. This idea of increasing the harvest potential of solar by way of surface geometry has been validated previously in [23, 24], but no analysis has been done by way of the cell orientation on the surface itself to optimize harvest. Geometry of the surface's cells need to be understood further because the simplicity seen in flat solar panels like homogeneous cells or arbitrary cell connections are no longer the case.

Concept of Morphology

For accurate potential harvest models, analyzing each unique surface is necessary to accurately simulate the energy harvest potential. Morphology is the characterization of a nonplanar surface mathematically by way of meshing strategies where the mesh faces are the PV cells to be fabricated. Much like a differential analysis is used to model the characteristics of an arbitrary surface[25], the surface will be partitioned into many smaller sections of area. In this process the size is restricted to a practical area for each partition. Figure 2 is a representation of the projection process being implemented where the curved surface will be approximated by a cell of planar dimensions. The mesh is generated to approximate the surface curvature of the nonplanar to accurately model the harvest potential. Gathering the individual characteristics of the surface was not necessary for flat plates since the normal and area of each cell were all the same. Individual cell characteristics such as normal and area or paramount for computing the harvest. After the surface is analyzed on an individual cell basis, a global harvest can be validated.

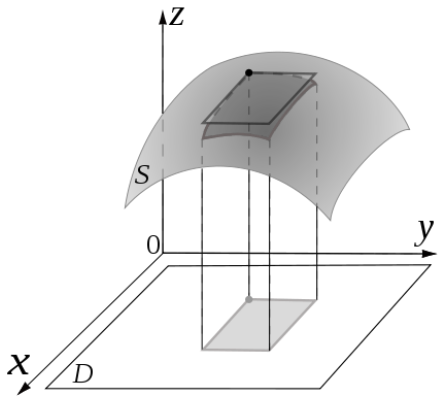

Figure 4: Footprint projection on curved surface

Investigating the characteristics of a nonplanar also forces a look into the effect that mesh geometry plays of the harvest. It is intuitive that meshing larger rates of curvature results in smaller cell sizes for a better approximation of the surface, but with this reduction in cell size the production capabilities are diminished proportionally. Morphology also serves to investigate this balance between mesh cell sizing with respect to curvature and maximizing harvest. The computations of this approach are modeling the theoretical maximum that the nonplanar surface can produce. Once optimized, further analysis into the electrical production and losses can be computed for use in the pixelization method in hopes to diminish the negative effects of mismatch current.

Concept of Pixelization

Pixelization is the act of grouping homogenously producing cells and determining appropriate cell interconnections to minimize the effect of cell mismatch. A group of cells that are similar in electrical operation characteristics can be called a pixel. Having analyzed the harvest potential of the surface in morphology, the pixelization approach will identify the most similarly producing cells and design them as one series connected array. Partitioning cells into pixels minimizes the variation in current densities within each array.

Conventional PV did not require this since all cells produced the same current densities due to their homogeneous surface characteristics. Each cell could be arbitrarily series connected and production would not change, assuming clear skies. This same interconnection on a nonplanar surface would have significant losses. With unique cell production characteristics, the pixels would determine a series connection of minimal

current mismatch. Once the pixels are determined, the information will be the design parameters for developing the PV system. This is integral to the ability to practically designing interconnections between cells such that the maximum power point tracking (MPPT) controllers can effectively condition and optimize the output.

Previous Works

Work has been previously conducted to validate the promise of intentionally nonplanar surfaces. In [23] a nonplanar PV setup provided 20% more harvest than that of a flat plate with the same planar footprint. Analysis comparing multiple nonplanar topologies and a flat plate in [24] was also done and in all cases the nonplanar surface harvested more energy. Others proposed a method for generating geometries for flexible PV modules on curved surfaces, finding the method designed appropriate cells to model the surface but noted the need for an approach for mitigating the mismatch produced [26].

Connecting the two approaches requires electrical PV models of which there are many. The ideal single diode model (ISDM) requiring extraction of only solar generated current, the diodes saturation current, and the ideality constant[27]. Although basic, insight can be gleaned about the inner workings from this simple model. The simplified single diode model (SSDM) includes the effect of the apparent series resistance(Rs) seen in every PV cell[28], increasing the computation needed. The series resistance is due to the contact resistance of the metal with the p- and n-layers, resistances of the p- and n-layers, and the resistance of the grid[29]. It is also highly dependent on the manufacturing process of the cell. Other factors like temperature can affect this resistance[30]. The single

diode model (SDM) is the most widely used model to predict the output of a solar cell, which includes the parallel resistance(Rp). This factor is a result of the leakage current of the p-n junction of the solar cell as well as the manufacturing method used [25]. Since, it is the most widely used model optimizations continue to be made, creating the improved SDM[31, 32]. More complex models like the two diode model(TDM) have also been investigated and were found to be more accurate but with a significant increase in complexity[33].

These models only account for the action of the solar cells. Parameters associated with the solar cell that are not given by the manufacturer are needed for accurate results. Depending on the model, there are unknown variables that need to be extracted for the computation of the electrical characteristics. In the SDM there are 5 parameters that need to be extracted Rs, Rp, A, Io, and Ipv. There are many mathematical methods researchers have been investigating to compute these parameters for crystalline silicon[34-38]. Extensive work has gone into this process because there is not one universally optimal method. Parameter extraction using genetic algorithms[36] or a mutative-scale parallel chaos optimization algorithms[39] are among some of the most interesting approaches produced from the need to accurately characterize a solar cell. Predictive models have also been proposed to using test data to derive the specific module parameters [30]. As modeling is material specific there are models that are more directed toward different types of materials like polymer solar cells, or events like local defects which act like additional parallel resistances[40]. These methods were reviewed and considered for the method requiring $i - v$ characteristic curves.

Once the parameters are delivered from the model, the electrical production must be harnessed and conditioned into usable power. This is done by the MPPT algorithms of the power electronics side. The output of the pixelization method would be implemented by the MPPT controllers such that each pixel would need a controller. MPPT can be categorized into two areas improved techniques and improved topologies. In [41], a review of MPPT techniques was done and was comprised of model based, model-free, and hybrid classifications. The most known method is perturb and observe method is a model-free method requiring only measurements of the system, but has issues oscillating at steady state[42]. Depending on the complexity of tracking needed, these techniques have been developed to work with multilevel inverter topologies as well[43, 44]. Although not addressed in this thesis, the ability of integrating the PV system to an appropriate inverter topology is paramount in any practical application therefore a review of current technique parameters was necessary.

Radiation models, electrical models, and MPPT techniques have been investigated. All the works reviewed are notably beneficial to the advancement of practical thin-film systems. The proposed method, a tool designed in hopes to coordinate all these aspects, will be presented along with the results and issues found during the analysis.

CHAPTER II

PROBLEM DEFINITION

Photovoltaic systems were investigated and engineered under the assumption that solar cells are and restricted to a flat form factor and are homogeneously producing generation sources, assuming no shading is present. With the advancements in the photovoltaic materials there is now precedent to reevaluate the approach to photovoltaics. No longer are solar panels limited to a planar form factor. BIPV for architecturally aesthetically pleasing features is now a possibility. Integration on to barrel roof tiles, domed roofs, curved walls, or even tents are other possible applications. Since implementing solar on any surface is now doable, it suggests the need to investigate the issues accompanying nonplanar PV. The research will shed light on the additional issues and complications associated with their applications. The two major hindrances are the light gradient over any given surface and the coordination with the power electronics to properly condition the raw production.

View Factor Gradient

The concept of view factor has been used predominantly in the study of heat transfer. Heat transfer has four distinct mechanisms conduction, convection, thermal radiation, and phase-change transfer[45]. Solar harvesting depends on the radiation transfer from the sun to the collector, so thermal radiation becomes relevant. View factor is the cosine angle of incident light exposed to the area of any given surface, depending

only on geometry. View factors have been used to effectively calculate the harvest of irregular surface[46]

Radiation can transfer heat through any transparent medium. This transfer of thermal radiation is caused by the transmission of electromagnetic radiation theoretically described by the black body theory. A black body is a perfect emitter and absorber of radiation. Radiative heat transfer laws suggest that a view factor is proportional to the radiation that leaves one surface and strikes another [41], expressed in figure 5. Two flat differential areas are representative of the sun and earth, separated at a distance S. θ_1 and θ_2 are the angles between the normal and direction of the ray. When a relatively infinite distance between surfaces like the earth and sun, the view factor can be considered to be a proportion of the projected and actual area as observed by the sun's position. From this realization, the view factors exist in a closed set of real values [0-1]. '1' is indicative of radiation vector is equal to the normal of the surface, described as a 0°. A view factor of '0' describes when the radiation does not strike the surface, described as an angle of 90°. For every position of the sun as radiation strikes the surface, relative to the collector, there is an angle of incidence at each differential area on the surface that results in a view factor, giving a proportion of radiation by the surface. For example, if 1000 W/m^2 radiated down at a surface with a view factor of 0.5, it would only be able to harvest half of what is present.

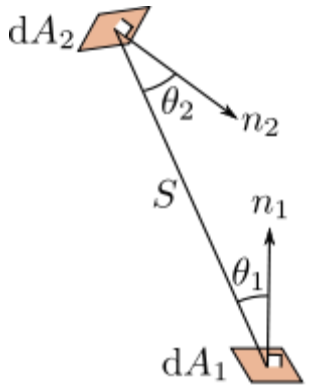

Figure 5: Representation of view factor using black body theory

For a nonplanar surface the view factor is changing relative to the position of the sun and orientation of the area. Analysis needs to be run for each cell to approximate the surface. A nonlinear surface would produce a nonlinear progression of average view factors as opposed to the linear change of a planar system. Figure 6a visualizes the average view factors of a flat plat with respect to solar hour and it results in a linear transition of values. Figure 6b is a nonplanar surface average view factor representation showing a nonlinear trend. The flat plat varies from 90° to 0° whereas the semi cylinder varies between 75° and 45°. Although the flat plate reaches the best view factor of 0°, it also reaches the worst. Taking into account the added area of the nonplanar, there is reason to expect larger harvests at hours where the flat plate production would be negligible. This nonlinear trend does, unfortunately, complicate the analysis but can be overcome through individual cell characteristics for precise knowledge of the surface.

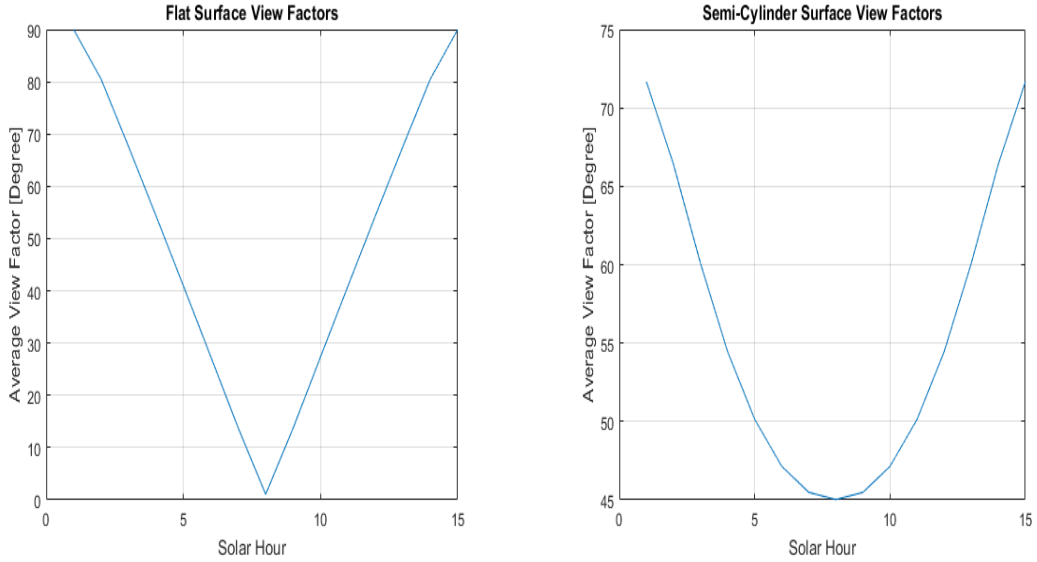

a) **b)**

Figure 6: Comparison of average view factors between a) planar and b) nonplanar surface

Mitigating Current Mismatch

There are two main causes of current mismatch in conventional c-Si solar arrays material degradation and shading. Shading of one cell in a series connected array can drastically drop the resultant output current. The cell responds by acting like a reverse biased diode, thus limiting current from flowing through the rest of the cells in the array. As a result, hot spots are generated from the circulating current in the shadowed cell[47]. This circulating current dissipates generated power internally and causes irregular $i - v$ curve characteristics which serves to further complicate the MPPT method needed as see in figure 7. Figure 8 represents the apparent current flow in shaded system. For BIPV partial shading and diversity of tilt angles are the main causes of mismatch. Yet, in some situations these varying panels are connected to the same inverter[20]. This mismatch

resultant from shading or varying tilt is synonymous with the issue presented with nonplanar thin film applications. It is necessary to determine the most similarly producing cells to minimize mismatch, otherwise the cost will not outweigh the benefit of the nonplanar system.

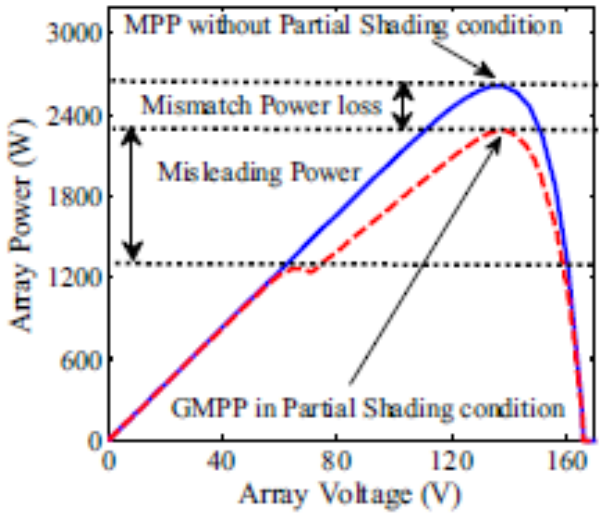

Figure 7: Power vs voltage characteristic with and without shading[48]

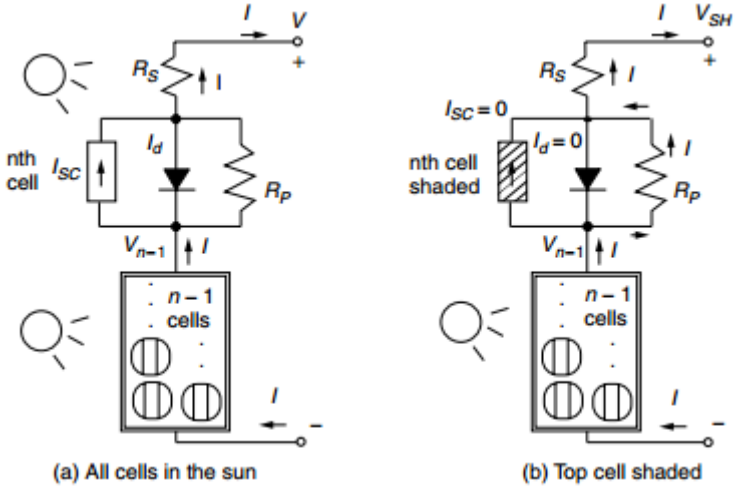

Figure 8: Current path for solar cells with and without shading[48]

CHAPTER III

MODELING APPROACH

This chapter outlines the steps taken to appropriately model nonplanar solar surfaces. The first section describes the morphology of the surface, used as a base for the extraction of the electrical characteristics. Once the electrical component is simulated, the results are then used in the proposed pixelization method in hopes to minimize the generated current density mismatch. This process has been designed to facilitate the dynamic nature of nonplanar PV and is proposed as a functional tool.

Software Review

The goal attained in this section of the approach was determining the view factors associated with a specific nonplanar surface. The first step in determining these view factors was selecting an appropriate meshing software that would allow for maximum accuracy of the curved surface. After the review of software options expressed in table 1, Gmsh was selected as the most geometrically comprehensive software to use.

The open source software Gmsh was the initial platform from which the meshed surfaces were generated for use in MATLAB for computation. Figure 9 demonstrates the initial process in the beginning of this research. The first step was to design the surface with the Gmsh interface in order to more accurately refine the geometry of each cell as well as overall surface approximation.

SOFTWARE PACKAGE	SCOPE OF MODELLING	EASE OF INTEGRATION	LIMITATIONS	COST
MATLAB	Mesh Design Electrical model Thermal model Optimization Plotting and reporting	All aspects of the modelling can be done in MTLAB 3rd party add-ons available for specific meshing designs	Unable to generate mesh with desired geometrical features Issues implementing arbitrary surface	Expensive Free Student Access
GMESH	Dynamic Generation Calibrate Parameters High Order Meshing Refine Design Optimize Geometry Calculates Error	Data can be transferred to MATLAB manually 3rd party libraries are available for alternative integrating techniques	Only designed for geometric blocked meshing	Free due to GNP General Public License
Mathematica	Delauny mesh Voronoi mesh Convex Hull mesh, etc.	Integration with MATLAB by way of ToMatlab.m	Rigid meshing techniques	Expensive Free Student Access
COMSOL	Moving Mesh with ALE Meshing and FE types Geometry Modelling	COMSOL with MATLAB option	Designed to be end result Rigid meshing techniques	Expensive
ANSYS	All meshing settings can be selected	Data can be transferred to MATLAB manually	No designation of meshing technique implemented	Expensive

Table 1: Descriptions of reviewed software packages readily available

The idea was to extract this generated mesh data and integrate the surface characteristics into the MATLAB for the algorithms to determine the absolute energy harvest capabilities. For this to work the transfer of data from Gmsh to MATLAB needed to be structured appropriately, meaning the user must extract only the data required to plot in MATLAB. Work was done to extract the specifics required out of the .msh file format generated by Gmsh. Initially, it was found that as surfaces or mesh techniques change the in the Gmsh platform the algorithm also needed alterations. Although this platform was appropriate for the necessities of implementing various meshing techniques as well mesh validations, it created significant integration problems.

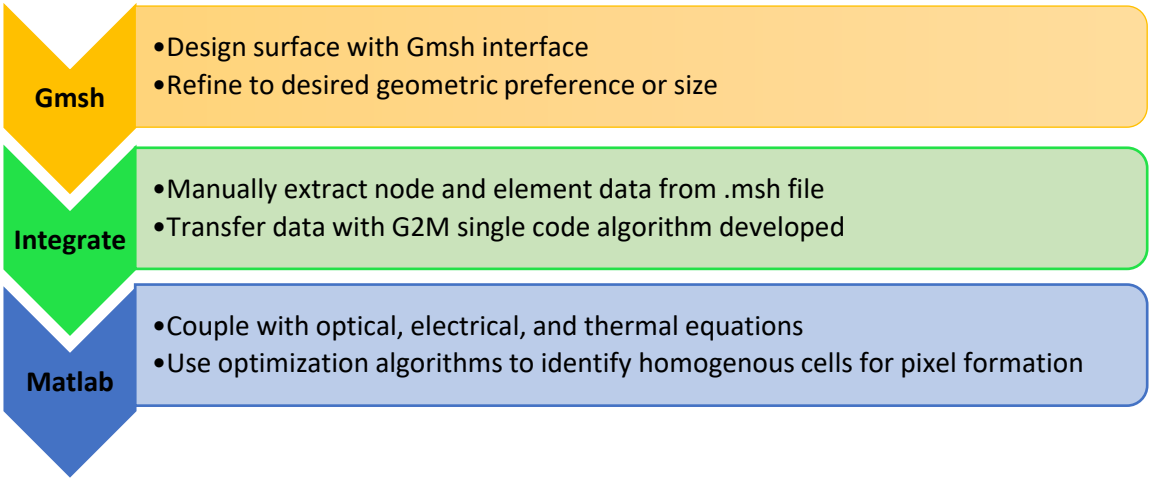

Figure 9: Workflow for integrating Gmsh with MATLAB

Once integration was achieved extracting the vertex data there were still issues left to overcome such as edge generation and surface orientation. Thus, to mitigate this issue of data transfer it was found that MATLAB was more appropriate for this phase of research. The MATLAB platform has sufficient functionality to create these non-flat surfaces.

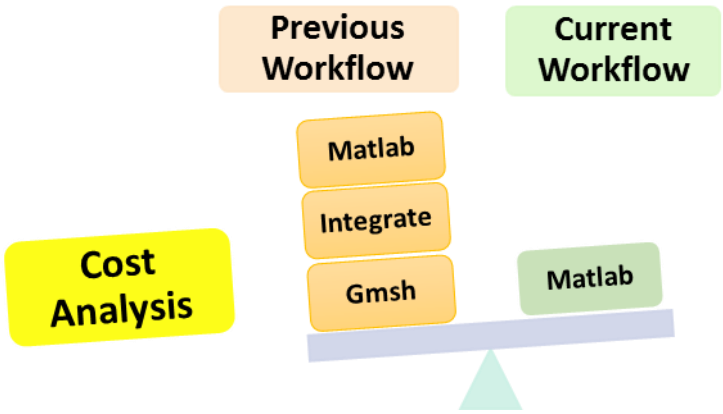

Figure 10: Cost analysis on software selection

Generating Nonplanar Surfaces

In order to validate the difference in potential energy harvest of nonplanar surfaces various surfaces that are representative of solar cells were created. As reviewed in the previous section it was found that MATLAB was the most practical approach to generate these meshed surfaces. Various surfaces of increasing complexities were reviewed. Geometries like semi-cylinders, ellipses, sinusoids, and even cones were created to analyze the effects of nonplanar surfaces.

These surfaces with normalized bounds were specifically selected by their limited degrees of freedom (DOF). DOF can be easily understood as the axis of rotation of the surface. For a flat plate there is no curvature, thus it has 0-DOF. Alternatively, the semi-cylinder and hemisphere have non-zero DOF. The semi-cylinder surface rotates about only a single axis, meaning that it has only 1-DOF. The hemisphere surface is geometrically synonymous with a rotation about two axes resulting in 2-DOF. Additional degrees of freedom increase the complexities of the computations as well as the indexing of the mesh cells for troubleshooting. The algorithms of this research have been designed to be compatible with that of 0-1 DOF. For 1-DOF surfaces, the x-axis was designated the axis of rotation. This was necessary to designate for cell index coordination.

Before moving forward with the modeling, a surface mesh geometry needed to be selected. A rectangular mesh cell structure on each surface was designed. The decision to implement this mesh structure was made due to the complexity of referencing the surfaces. It is paramount that the data is tracked appropriately as each cell could possibly contain unique attributes compared to adjacent cells. An additional benefit to using a rectangular

mesh rather than a triangulation was to increase the surface area of each cell which increases the practical harvest by reducing manufacturing and interconnections necessary. As shown in figure 11, the indexing method implemented requires a specific direction of cell generation in order to keep track all the associated data.

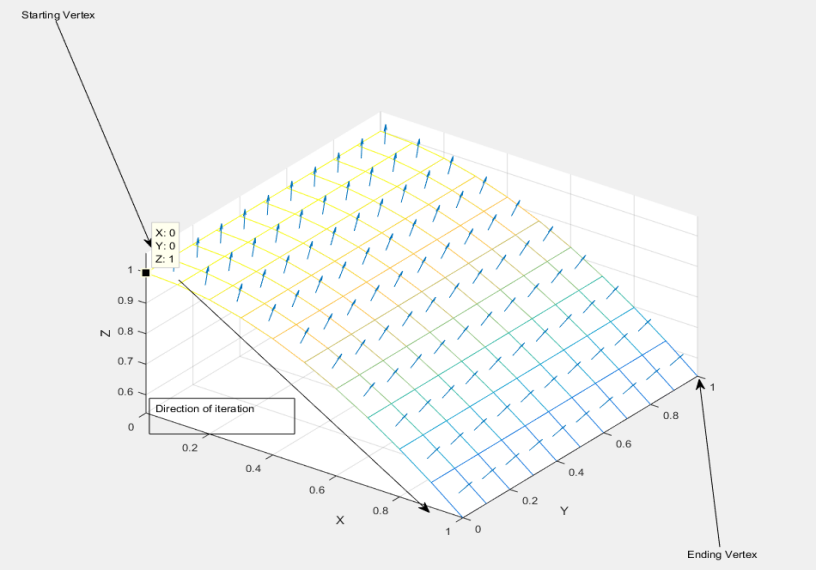

Figure 11: Indexing layout for generated surfaces

To create surfaces in Matlab the function *surf(X,Y,Z)* and *mesh(X,Y,Z)* were implemented. *Surf(X,Y,Z)* plots a surface such that X and Y represent the effective footprint plane and Z is indicative of the height of the surface. X and Y are represented as vectors such that length(X) = m and length(Y) = n, thus size(Z) = [m,n]. The generation of a flat plate is intuitive such that X and Y represent the footprint of the surface and Z is a constant value. For more complex geometries with non-zero DOF we alter this Z value

for each combination of X and Y, altering the dimensions of each cell face. With this added complexity, it emphasizes the necessity to track and index the data as it is transferred from the first stage of morphology to the electrical characteristic extraction of the second. As surface complexities are increased it is evident that a clear understanding of these algorithms is necessary. The MATLAB algorithms for generating these surfaces are shown in APPENDIX A.

Each surface mesh face is representative of a single solar cell to be analyzed. Figure 12 shows examples of the nonplanar surfaces to represent possible practical uses in these shapes. These figures are ordered in increasing complexity beginning with the flat plate. Recalling the normalized bounds, these surfaces can be scaled as necessary for practical applications. Also since the view factor calculations take into account direction and not dimension, this is possible. The varying rates of curvature are one aspect to be aware of. It is known that complexities arise with curvature, but rate of curvature of a surface may have more of an effect. These surfaces were selected to investigate this variable factor as well as the overall of practicality of solar modeling.

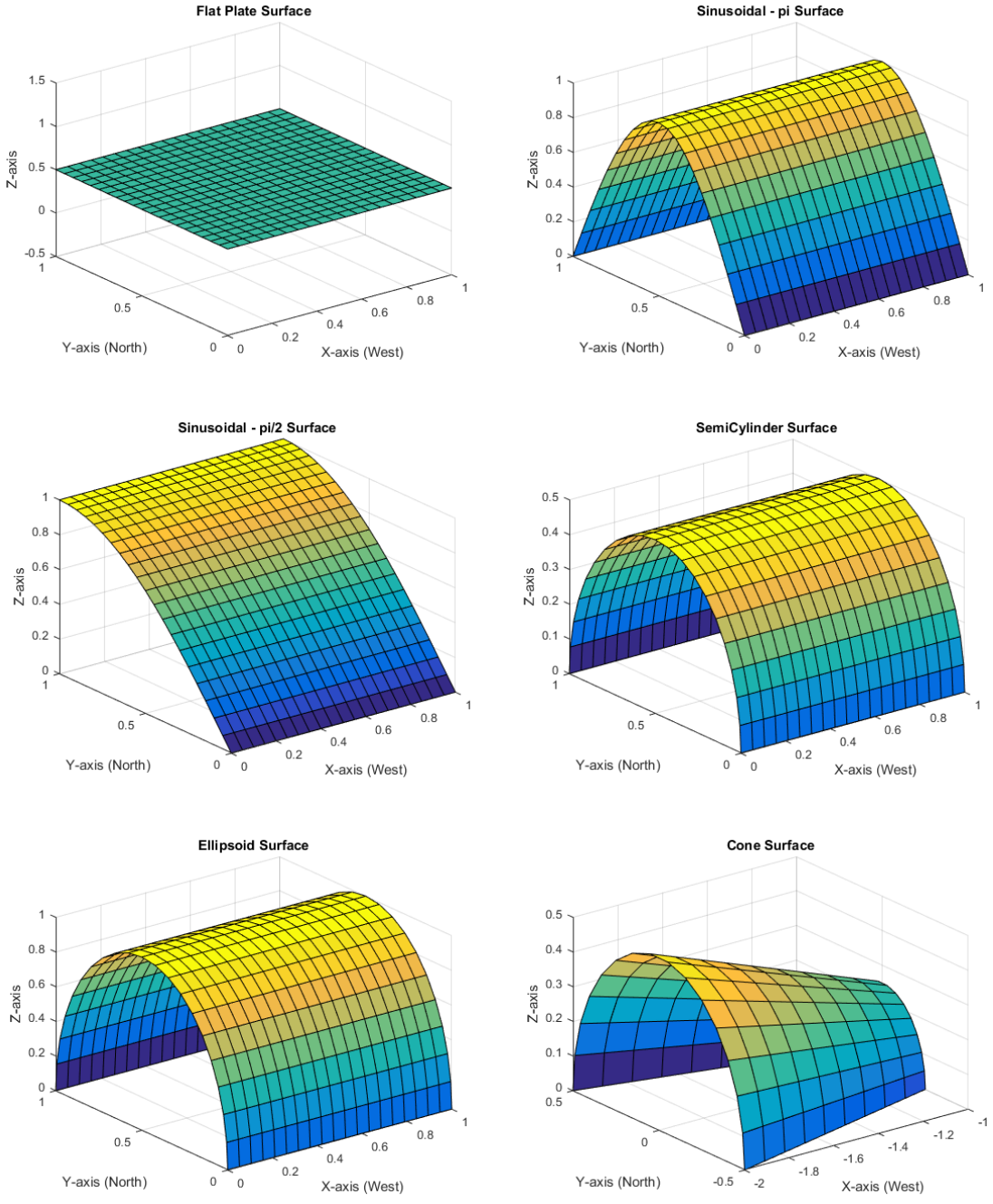

Figure 12: Various figures generated for analysis with the proposed approach

Morphology

Recalling from the previous chapter, morphology is the characterizing of the surface in order to better understand the dynamic effect on potential harvest. The most influential characteristic of the simulation would be accurate normal depiction of the nonplanar surface. Conventional solar panels are flat creating homogenous normals from the full surface, thus each individual cell. But for nonplanar surfaces, the apparent normals are no longer pointing in the same direction at various sun positions. The MATLAB function surfnorm(X,Y,Z) determines the normal at the vertices of the meshed surface. This is not appropriate for determining the exact normal of the cells under analysis. A normal correction was needed in order to more accurately represent each cell. Surfnorm(X,Y,Z) outputs vector components U, V, and W of the vertex normals. U, V, and W represent the X,Y, and Z components of the normal vector respectively. Understanding this convention is necessary for correcting the normals for each cell. The normal components of the four vertices depicting a cell face are averaged together in order to correct the error. In small rates of curvature this correction is less apparent. Alternatively, in high rates of curvatures like a peak of a sinusoid it is much more significant. Figure 13 shows the effect of this correction on a sinusoid. The peak of the surface is shown at the highest rate of curvature, depicting a more significant adjustment than the smaller rate of curvature of the adjacent cells.

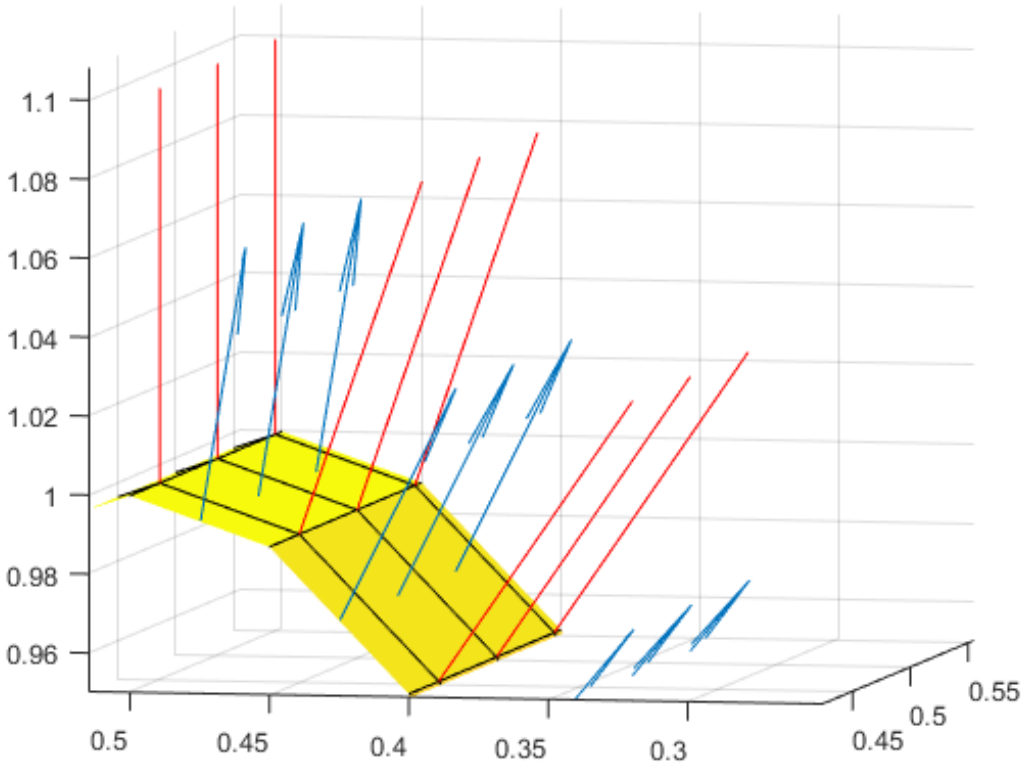

Figure 13: Corrected cell normal compared with original vertex normal

Furthermore, figure 14 shows the correction on a semi-cylinder surface with respect to the originally generated normals. Figure 14a depicts the V-vector component correction of the normal component of a single cell at each sun position, effectively the x-axis correction. The solid line represents the original value of the normal and the '*' depicts the adjusted value. Notice for the V-vector the largest correction appears at the highest sun position, or solar noon. For the W-vector, or z-axis correction, in figure 14b, the largest correction appears at the morning and evening solar positions.

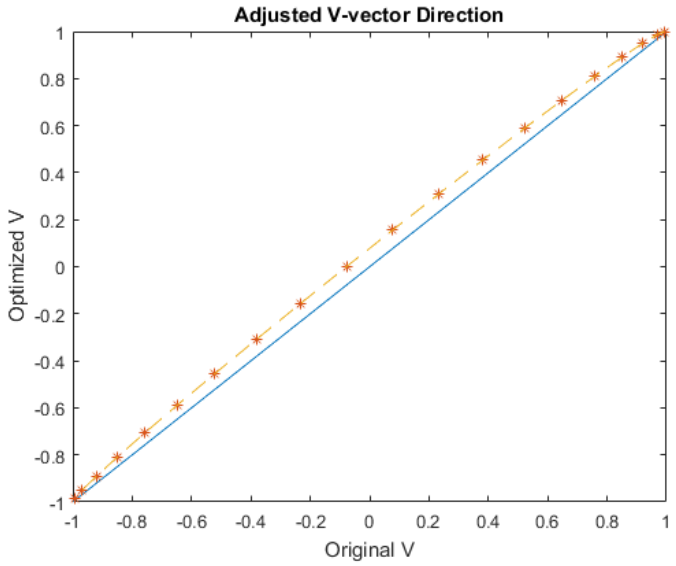

a)

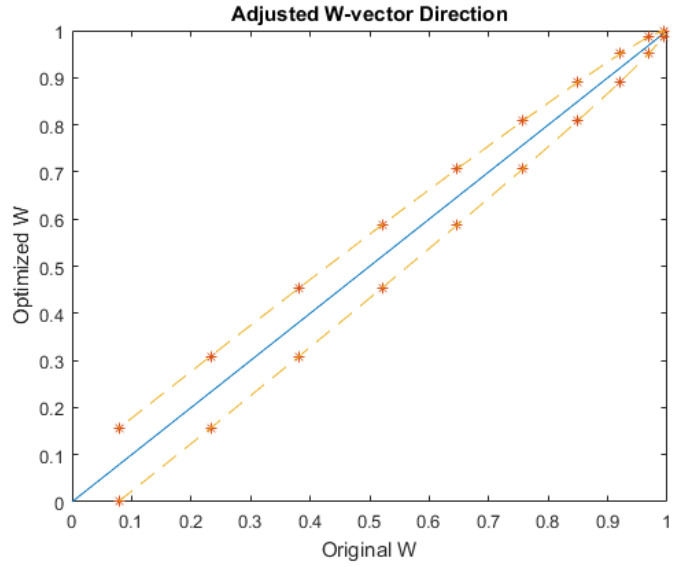

b)

Figure 14: Normal correction of the a) V-vector and b) the W-vector directions

The next aspect of morphology is to use the position of each individual vertex generated by the surf(X,Y,Z) or mesh(X,Y,Z) function to determine the center and area of each cell. Center data is used to position the normal of each cell as seen in figure 15.

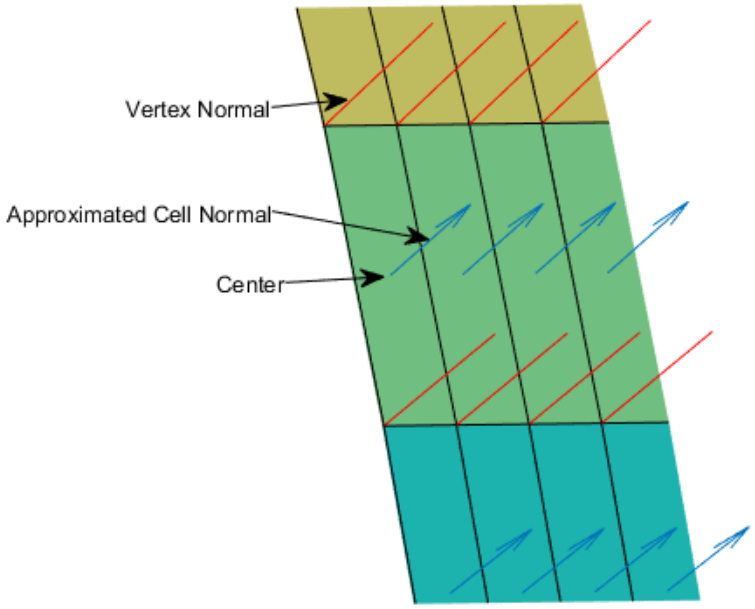

Figure 15: Positioning of the normal at the center of each cell

Each cell center is determined by again taking the average of the four vertex points that represent each cell. This is valid for only rectangular surface, thus another validating reason to use rectangular meshing, stated previously.

The area of each cell can also be calculated with the vertex data. The length, x-axis distance, is kept constant due to the decision to rotate about the x-axis for 1-DOF figures, meaning as you travers the x-axis the z-position remains constant. On the other hand, if you traverse the y-axis the z position changes. This height change with respect to the y

position introduces more variation in the computations. Figure 16 demonstrates how the footprint width of the surface that was introduced in the generation of the surface is not the actual width of the cell. The active width is needed to determine the actual area of each cell using the Pythagorean theorem. First the three-dimensional Euclidean distance is needed. This distance is calculated by equation 1 where AB is the distance between the two points under analysis. The area of each cell is then calculated using this active width. By computing the surface characteristics, it is also possible to include the size difference between surfaces which is useful for a cost-benefit analysis in practical real world applications.

$$AB = \sqrt{(x_2 - x_1)^2 + (y_2 - y_1)^2 + (z_2 - z_1)^2} \qquad \text{Eq. 1}$$

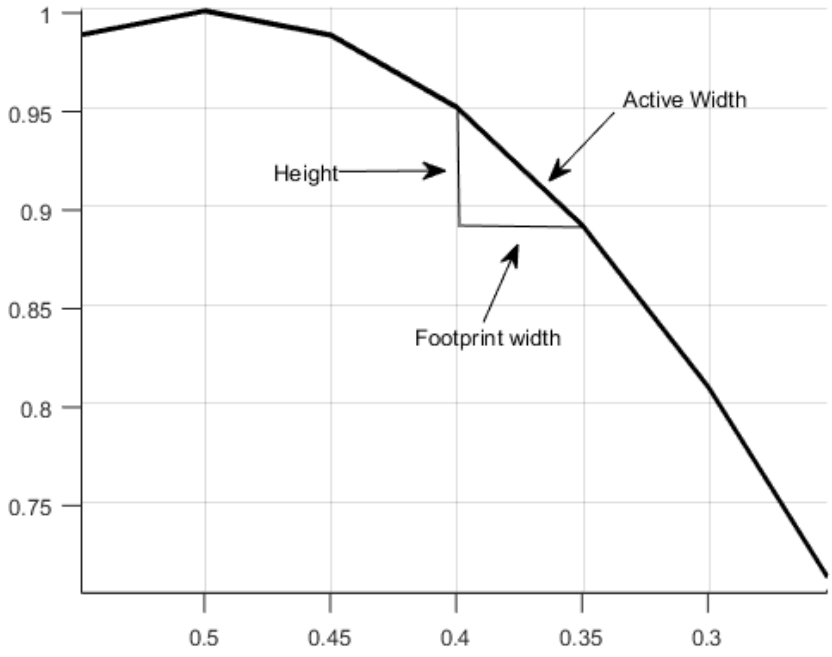

Figure 16: Active width vs footprint width on nonplanar surface

This process of morphology allows for analysis of arbitrary 1-DOF figures. Each unique surface will produce different distributions of cell normals and areas depending of the curvature of the surface. The surface data collected now needs to be coupled with the position of the incident solar irradiation in order to extract the theoretical harvest potential.

Sun Position

There are several ways to track the sun on any given day. In this work the sun position is described by two polar coordinates denoted by the azimuth angle (***ϕ***) and altitude angle(**β**). These coordinates depend on the latitude(**L**), day of the year (**n**), and the time of day. Figure 17 displays the orientation of the sun with the azimuth and elevation angle components. The following equations are used to calculate the solar positioning.

$$\delta = 23.45 \sin\left[\frac{360}{365}(n - 81)\right] \quad \text{Eq. 2}$$

$$H = \left(\frac{15^\circ}{hour}\right) * Hours\ before\ solar\ noon \quad \text{Eq. 3}$$

$$\sin\beta = \cos L \cos\delta \cos H + \sin L \sin\delta \quad \text{Eq.4}$$

$$\sin\phi = \frac{\cos\delta \sin H}{\cos\beta} \quad \text{Eq. 5}$$

$$if \quad \cos H \geq \frac{\tan\delta}{\tan L} \quad then\ |\phi| \geq 90°;\ otherwise\ \ |\phi| > 90° \quad \text{Eq. 6}$$

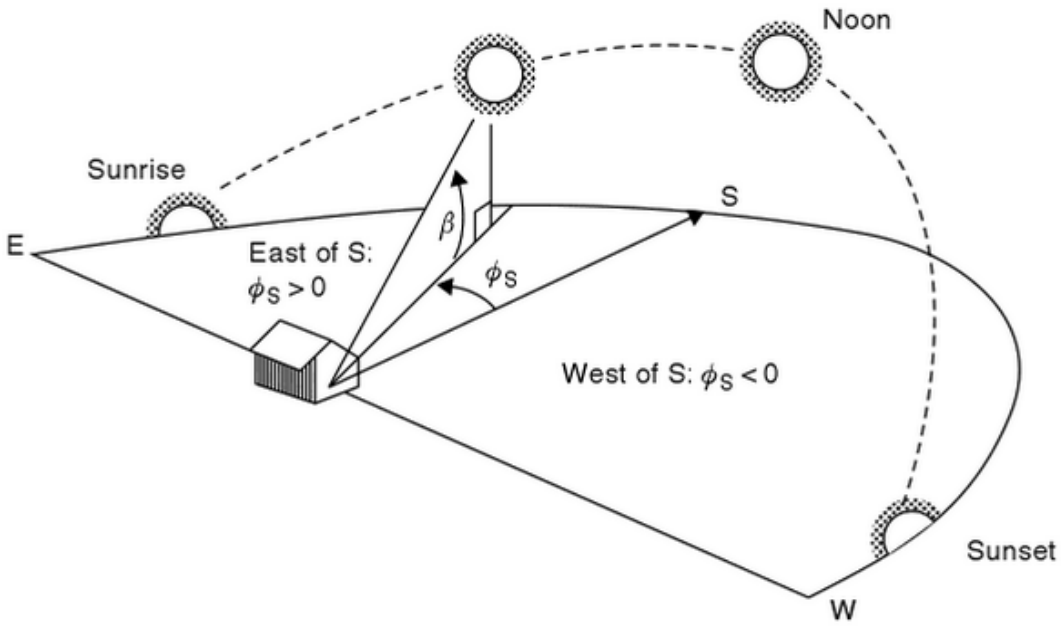

Figure 17: Azimuth and elevation angles with respect to the sun path [48]

There are many ways to visualize this sun position in Matlab. Using the surfl(X,Y,Z,**ϕ**,**β**) function or even the light(**ϕ**, **β**) function, the generated surface receives a gradient light effect. This gradient of light is dependent on the incident radiation that is seen by each cell face. The angle of incidence can be computed by the following equation where a represents the cell normal and b represents the vector components of the sun at a selected position.

$$\cos\theta = \frac{(a_1 b_1 + a_2 b_2 + a_3 b_3)}{\sqrt{a_1^{\,2} + a_2^{\,2} + a_3^{\,2}}\sqrt{b_1^{\,2} + b_2^{\,2} + b_3^{\,2}}} \qquad \text{Eq. 7}$$

Now that sun position and angle of incident are found it is important to determine the intensity of the radiation that is hitting each cell. This intensity is determined by the

distance of the sun from the earth, apparent extraterrestrial irradiation, air mass ratio, and the atmospheric optical depth. The calculations for determining the approximate intensity of direct beam radiation reaching the earth's surface are given below.

$$A = 1160 + \sin\left[\frac{360}{365}(n - 275)\right] \quad \text{Eq. 8}$$

$$m = \frac{1}{\sin\beta} \quad \text{Eq. 9}$$

$$k = 0.174 + 0.035 \sin\left[\frac{360}{365}(n - 100)\right] \quad \text{Eq. 10}$$

$$I = Ae^{-km} \quad \text{Eq. 11}$$

Once intensity of the radiation striking the panel is known, insolation striking each cell can be computed. Insolation is dependent on the apparent radiation, the view factor of the surface, and lastly the orientation of the surface. For comparable analysis, each surface was set to face due south with no tilt at a latitude of 23.45° on the summer solstice. The insolation collected can then be calculated by the following equation.

$$I_c = I \cos\theta \quad \text{Eq. 12}$$

$$\cos\theta = \cos\beta\cos(\phi - \phi_c)\sin\mathrm{T} + \sin\beta\cos\Sigma \quad \text{Eq. 13}$$

Where cos(θ) is the view factor of the surface, or in one cell of the surface. Since computations have been done to calculate this view factor angle, the approximated insolation collected by each cell can be determined. By the equations the view factor has a direct proportionality to the insolation collected by the surface. This connection makes it straightforward when simulating the maximum theoretical energy harvest potential.

Azimuth and Tilt of Surface

Another aspect that was considered was the orientation of the surface. Although for analysis comparing shapes an orientation was designated previously, the ability to change the orientation of the surface is necessary for more practical situations where the orientation is already set. For conventional flat solar panels to achieve optimal harvest the flat panel needs to be tilted represented by T depending on geographical location. The azimuth angle, denoted by the angle between the surface face and south, can also be adjusted to achieve maximum harvest at the desired time of the day. These factors still play a large role in nonplanar depending on the surface itself. Some surfaces would benefit from adjusting the tilt, so it is necessary to have this ability incorporated as an option in the research. The individual approach to analyzing the view factors and incident angles on each cell allows for easy integration of the tilt and azimuth of the collector which was not a simple analysis prior to this work. Once the surface is generated the desired tilt and azimuth of the collector can be produced on the original generated surface, and the same full analysis can be achieved.

Initially the surface is generated with collector azimuth of 0° directing the surface south with a tilt of 0° keeping the surface horizontal. In all plots displayed the x-axis is oriented such that the value increases toward the south. The y-axis is oriented such that the value increases toward the east. This is consistent with all normalized plots for comparison. Figure 18 displays this orientation.

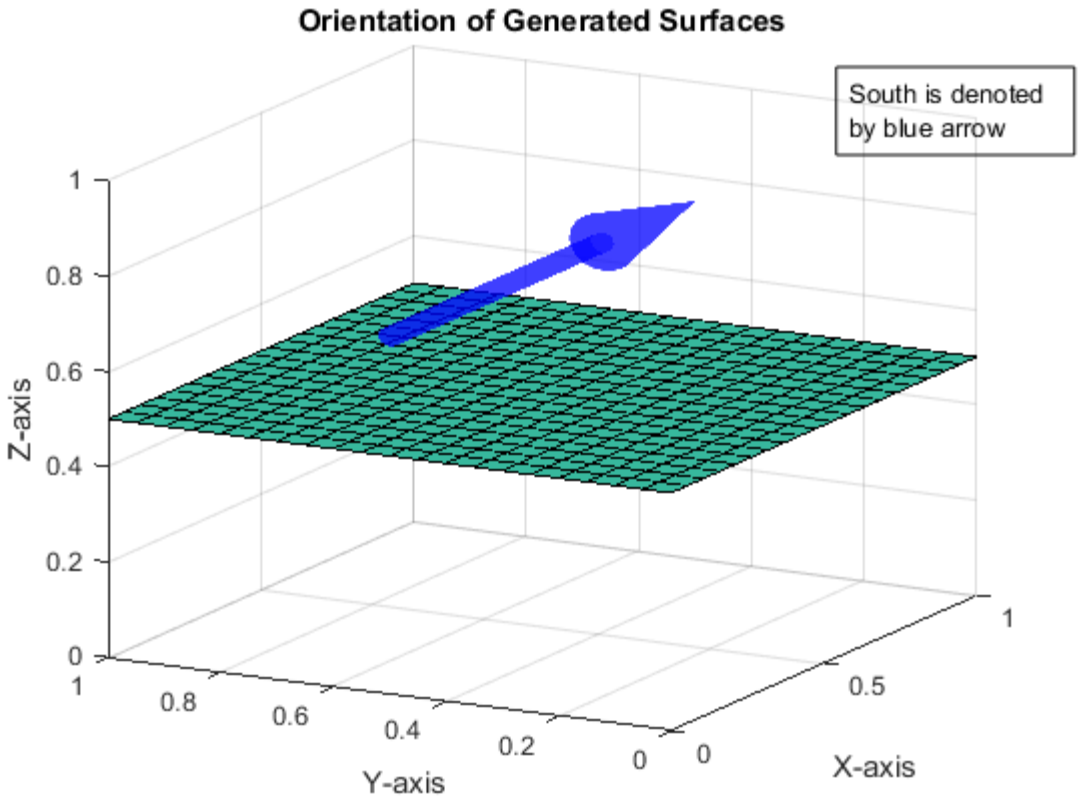

Figure 18: Orientation of the generated surfaces

Extraction of Electrical Characteristics

The next task is to extract electrical characteristics from the thin film material in order to integrate the insolation computed with the current density generated. Calculating the electrical generation per cell is of great importance for the MPPT. Current production depends on the insolation reaching the collector, the view factor of a cell, the area of the cell, material parameters, and usually unknown characteristic parameters that must be extracted.

The most basic model for solar is the ISDM, but with this it neglects many model parameters for simplicity. More exact calculations are desired so a variation of the SDM is used. Figure 19 shows the approximated circuit diagram of the SDM. Notice there are two resistances that are present in the model. This can be simplified because at such low voltage generation per cell the Rp value will be significantly larger that the Rs value, therefore the model is further simplified by neglecting Rp. This simplification brings us to use the SSDM that is mathematically modeled below. Ipv is the raw current generated by the solar cell. Io is the saturation current of Schottky's diode equation followed by the exponential term including the series resistance. Increasing Rs adjusts the slope of the open voltage side of the IV plot and in a more drastic way thus it was deemed necessary to include included in figure 20. V_t is the thermal voltage and a is representative of $\frac{q}{KT\iota}$ where q, K, T, and ι are the electron charge, Boltzmann constant, module temperature, and the ideality factor.

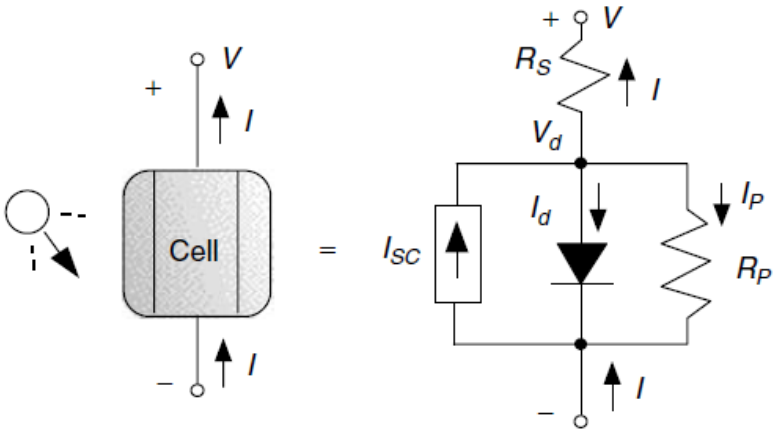

Figure 19: Single diode model of a photovoltaic cell [48]

$$I = I_{\mathrm{pv}} - I_0 \left[\exp\left(\frac{V + R_{\mathrm{s}} I}{V_{\mathrm{t}} a} \right) - 1 \right] \qquad \text{Eq. 14}$$

One complication with this equation is that it is a transcendental, requiring previous values of the output the determine the present value of current. The voltage range was determined by the data sheet provided by the manufacturer. This allows us to remove one of the variables in the system and compute $i - v$ characteristics with the Newton-Raphson method. Ten iterations were allowed for determining the appropriate output current. Insolation is directly proportional to the short circuit current as seen in the below equations. In addition, the temperature dependence was also included as it does affect the $i - v$ characteristics as well most notably at the open circuit voltage. Figure 20 displays the $i - v$ characteristics with respect to different temperatures of a specific cell on an arbitrary surface. As temperature increases the open circuit voltage is reduced. On the other hand, there is a very small increase in the short circuit current. This work addresses some of the most significant temperature factors of photovoltaic modeling.

$$I_{\mathrm{pv}} = (I_{\mathrm{pv,n}} + K_{\mathrm{I}} \, \Delta_{\mathrm{T}}) \, \frac{G}{G_{\mathrm{n}}} \qquad \text{Eq. 15}$$

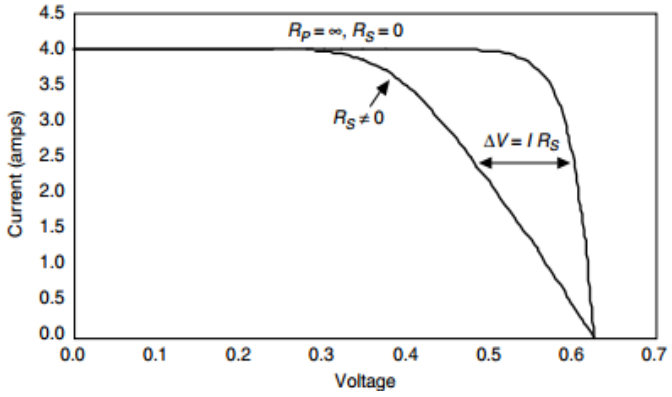

Figure 20: IV characteristics of a non-zero series resistance [48]

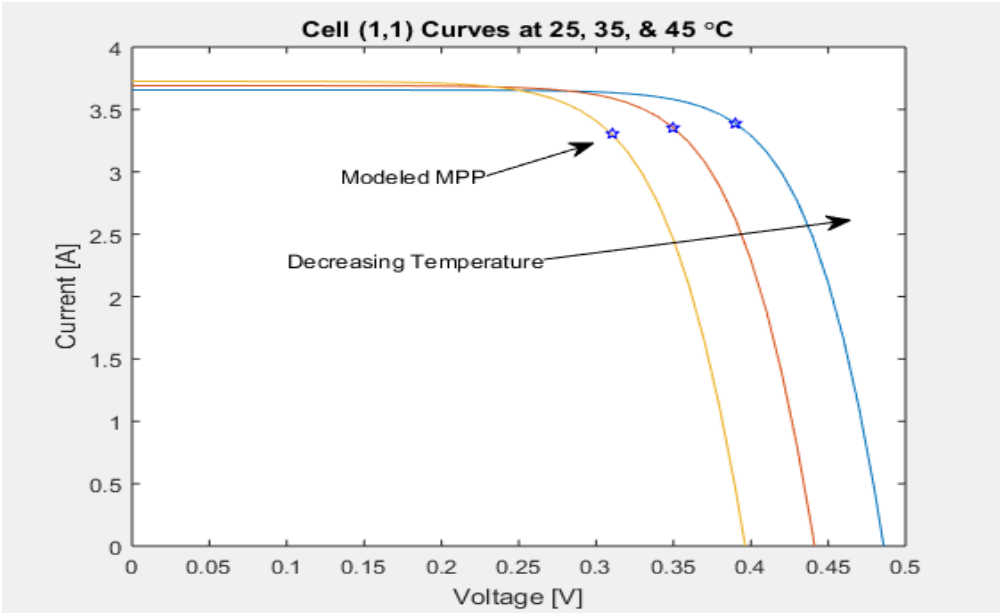

Figure 21: IV characteristics with respect to temperature changes

Pixelization

The last aspect of this approach is pixelization which is the grouping of homogenous cells. The simplicity of flat plate panels being arbitrarily interconnected is

no longer the case. This brings rise to the necessity of determining which cells are producing current densities that are similar enough to mitigate the effect of mismatch. As stated in the introduction this power loss through mismatch is synonymous with shading effects of flat place photovoltaics and remains one of the major disadvantages of using thin film photovoltaics on nonplanar surfaces. Unlike with flat solar panels, nonplanar surfaces are unable to connect the cells of the panel arbitrarily. Connecting a nonplanar surface in an arbitrary series fashion would lead to detrimental circulating current and inconsequential power. In order to maximize the harvest potential of a nonplanar surface one must connect each cell with its own MPPT controller. Each cell would be controlled to maintain its maximum power, but this is impractical due to cost, size, as well as added losses associated with additional connections for each cell. Thus, this work proposes performing a grouping algorithm on the simulated output current production of the material to find the balance between minimal MPPT controllers and optimal power output.

Clustering techniques have a wide range of applications such as biomedical research, pattern recognition, image processing, economic science, energy optimization in sensors, as well as environmental modeling[49-52]. Since there are numerous types and variations of these clustering methods it is paramount to find an appropriate technique to fit this mathematical modeling. The maximum power points of the $i - v$ curves were extracted from each cell to be clustered since this is the optimal output desired for each cell. The current data at the maximum power point specifically has the most impact. The current data given into this clustering algorithm will be only one dimensional, being only a single value, so it reduces the need for complex clustering techniques.

K-means clustering algorithm was selected as the most appropriate method to begin. K-means is an unsupervised numerical partitioning clustering method that is capable of selecting the desired clusters, denoted k. Determining number of clusters is vital when restricted to a certain number of MPPT controllers. K-means clustering begins by arbitrarily selecting starting position for k desired clusters. These starting positions are considered mean-vectors and act as a representative of the cluster as it gathers data points. As k-means iterates it evaluates distance between data and mean vector and assigns data to the closest cluster. Once a data point is assigned to a cluster, the mean-vector of that cluster is updated for the next iteration. This process continues until the data no longer moves to other clusters. Finding the closest cluster to a data point minimizes the mean-object dissimilarity by a Euclidean distance metric[49]. Below is the data flow for the k-means algorithm implemented by way of the *clusterdata()* function in MATLAB.

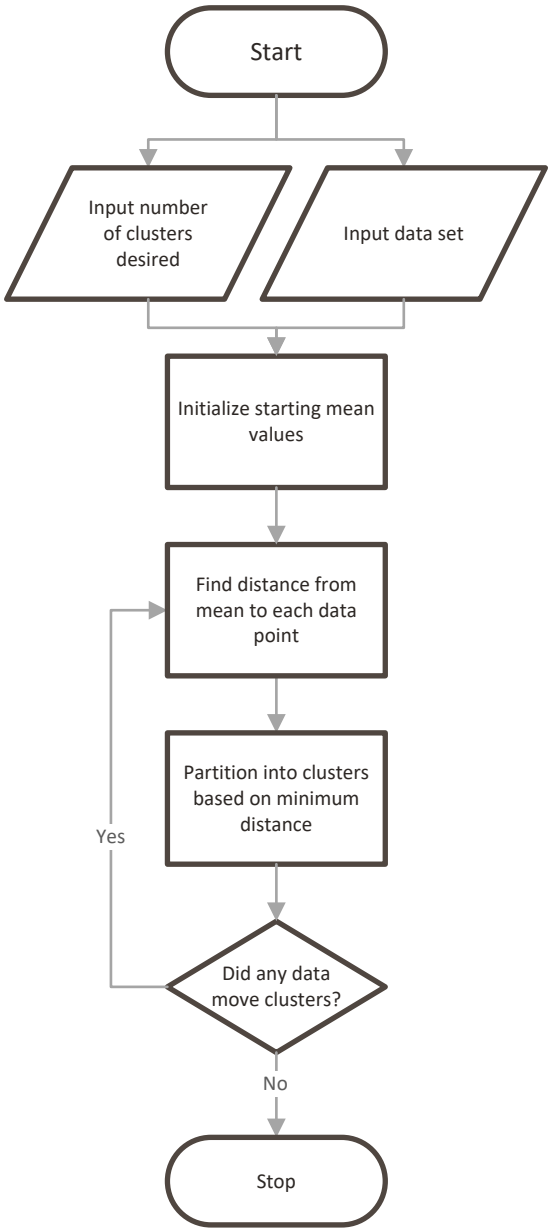

Figure 22: Workflow for k-means clustering algorithm

This proposed approach is an initial investigation of the practicality of using clustering as an optimization tool in nonplanar thin film photovoltaics. The K-means methods does have some drawbacks such as terminating at local optimums, effected by

outliers in data, and dependence on initial cluster position[53]. Although negatives are present, this process is an appropriate initial tool for optimization due to efficiency and relatively low complexity[53]. Distance and linkage are other parameters that will alter the functionality of the algorithm that must be addressed. The distance parameter is how the algorithm will compute the dissimilarities between objects to be clustered. The linkage parameters determine how the data is distributed into clusters. Average linkage is when the average of the data points in one cluster is compared to another cluster. Median linkage takes the median distance between all data points to determine the linkage between clusters[52]. They produce minor differences when compared with each other, but from initial analysis median linkage produce more practical groupings due to the strong effect of outliers.

K-means clustering algorithm was implemented for every spatial position of the sun in the analysis. The maximum power points are inserted into the k-means algorithm for clustering. At each sun position this approach will deliver the user defined number of pixels composed of cells to be series connected. This interconnection layout is optimized for this specific sun position. The optimal interconnection layout is dependent on the considered surface, requiring further consideration. Variations of post pixelization methods were used to determine the optimal layouts.

CHAPTER IV

VALIDATION OF MORPHOLOGY

This chapter serves to validate the morphology approach where the surface is characterized by way of a rectangular mesh to describe the potential harvest of the nonplanar surface while also maximizing harvest through mesh geometry. Each surface beginning with the flat plat is generated and characterized to extract the surface details, specifically the view factor gradient over the course of a day. With the addition of the insolation intensity and direction from sun path modeling the energy harvest can be computed. The solar position at each hour was extracted to analyze the surfaces. All cell production is accumulated to give the overall energy harvest plots. For comparison, the summer solstice or day 173 was selected for all simulations. All surfaces were given a latitude of 23.45° because on this day the sun is directly overhead at solar noon. The orientation of each surface was set facing due south with no tilt. The footprint area of every surface was restricted to a value of 1 square unit. This normalization allows for the scalability of the model.

Flat Plate Morphology

The flat plate surface is the reference to which other surfaces will be compared. Figure 23 shows the generated surface showing its associated normal alongside the energy harvest associated with it. In order to validate the morphology of a surface, the calculations on individual cells must coincide with the global harvest prediction. This requires referring to the view factor calculations with insolation direction and intensity calculations at a

specific sun position. An arbitrary cell on the surface was selected for analysis. The cell should represent all other cell in this flat plat evaluation. Knowing the solar position given by the azimuth and altitude angle as shown in table 2 the view factors of the surface can be calculated. A positive azimuth corresponds to an angle east of south whereas a negative azimuth is indicative of an angle west of south.

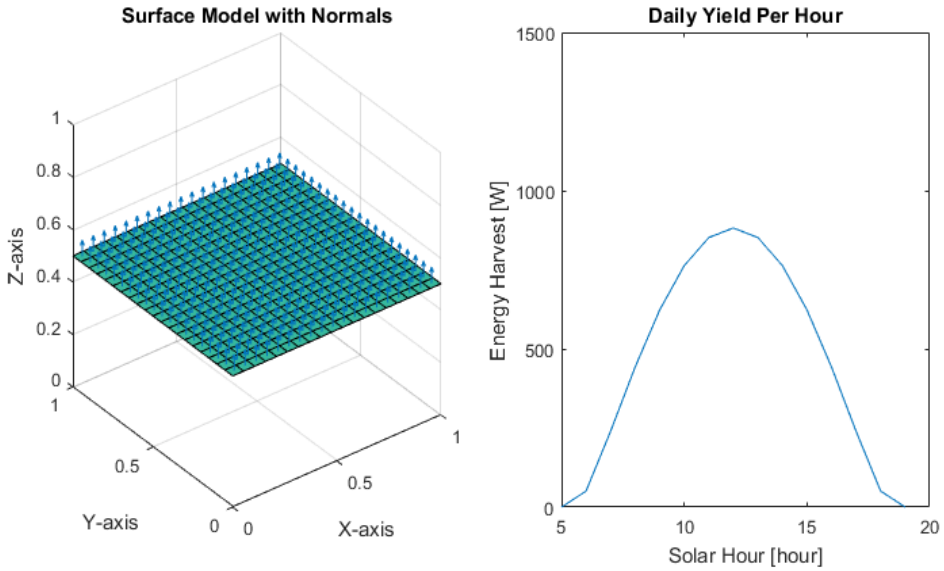

Figure 23: Flat surface model and potential harvest plot

Table 3 compares the view factor, area, and power generated at two positions of the sun. This validates that the individual cell calculation is an appropriate approach for modeling the solar harvest. The view factor is seen to be the same as all other cells on the surface which is validated by the understanding of view factor. The area is also correctly calculated and is proportional to the full surface. The power generated is proportional to

the full surface production and is consistent with the equations for insolation. For orientation changes, the view factors adjust accordingly due to the change of normals on the surface, thus it is valid although not expanded upon for this initial analysis.

Solar Hour	Altitude Angle (°)	Azimuth Angle (°)
5	0	117.6053
6	9.498	111.5382
7	22.4006	106.5671
8	35.6211	102.2059
9	49.0532	98.1646
10	62.6214	94.0665
11	76.2605	88.6983
12	88.948	0
1	76.2605	-88.6983
2	62.6214	-94.0665
3	49.0532	-98.1646
4	35.6211	-102.2059
5	22.4006	-106.5671
6	9.498	-111.5382
7	0	-117.6053

Table 2: Azimuth and elevation angles for the summer solstice at 23.5°

10:00 AM	Cell	Full Surface (380 cells)
View factor	0.888	0.888
Area (pu^2)	.0026315789	1
Power (W/pu^2)	2.00995	763.7817

12:00 PM	Single Cell	Full Surface (380 cells)
View factor	0.9998	0.9998
Area (pu^2)	.0026315789	1
Power (W/pu^2)	2.32299	882.7343

Table 3: Arbitrary cell characteristics at different solar positions

For the flat plate, as expected, in the morning hours the average view factor of the surface is very low corresponding to an equivalently low energy harvest potential. Peak harvest on the surface occurred at solar noon as expected reaching 882.7343 W/u^2 and the overall energy harvest was calculated to be 6802.1J over the course of the day from figure 23.

Pi/2 Sinusoid Morphology

The pi/2 sinusoid surface analysis in figure 24 shows similar results to that of the flat plat since it is the most similar of other analyzed surfaces. The amplitude of the surface was selected arbitrarily. The early hours of the day produce less compared to the flat plate. Also notice that the peak of the harvest is no longer centered at solar noon. The orientation of the surface being curved toward the west creates this result. The energy harvest begins later in the day because the incident light is not yet striking the area of the surface or has a very low view factor. The adjustment of the peak harvest resembles the effect that tilting the flat surface would have, but with more gradual descent from peak harvest. Peak output of the surface was 690.29 W/u^2 occurring at 2:00PM with a total energy potential of 6984.17 J both of which are larger than the flat plate.

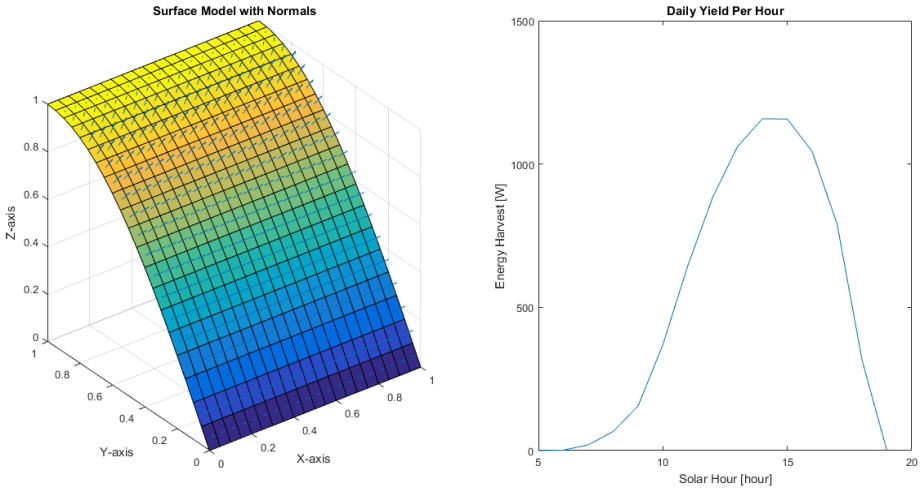

Figure 24: Pi/2 sinusoid model and potential harvest plot

Pi Sinusoid Morphology

The energy harvest modeled shows interesting results for the pi sinusoid figure. The amplitude of the surface was selected to be 1 arbitrarily. The power being generated rises and falls rapidly in the early and late hours of the day, and it flattens out for the mid-day hours. This can be compared to the pi/2 sinusoid where it peaks later in the day since it curves toward the west. For the pi sinusoid, it curves to face both east and west directions causing it to have local peaks of 884.3 W/pu^2 in the morning and the evening since the normals on each side are receiving approximately perpendicular incident radiation. The peak of 890.52 W/pu^2 seen at noon can be attributed to the sun being directly overhead. Light strikes every cell of the surface, resulting in a slight peak despite the poor view factors expected for much of the surface. Overall the harvest of this surface has a potential harvest capability of 9712.32 J on this day. The early morning peaks of power are

beneficial in applications that require starting potential. Motors require about 200W of power to start running and will drop once idle and would benefit from the early hour availability of power from this surface.

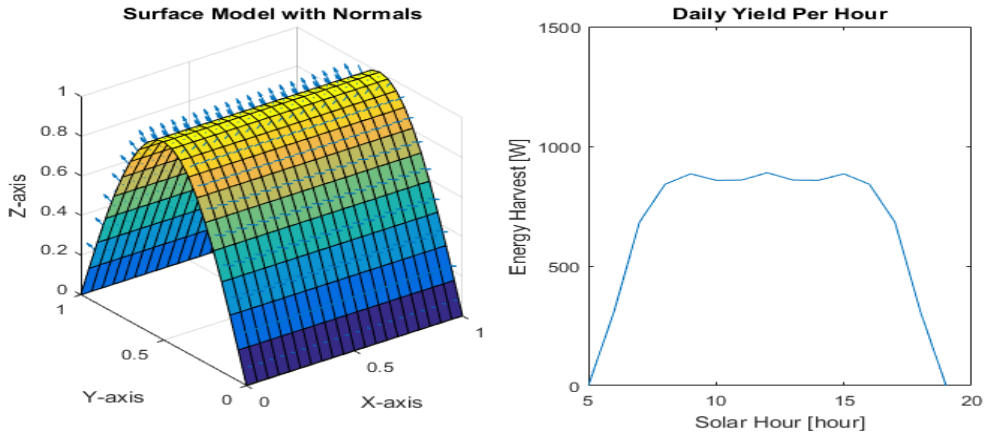

Figure 25: Pi sinusoid model and potential harvest plot

Semi-Cylinder Morphology

Like the pi sinusoid the semi-cylinder curves around the x-axis in both the east and west directions. The result of the simulation shown in figure 26 displays a very smooth increase and decrease of energy over the day. Compared with the flat plate the semi-cylinder shows higher collection in the morning and evening this is caused by the view factor being higher in this case for those solar positions. The peak power of the harvest was 882.9796 W/pu^2 at noon while the total energy harvest over the day was calculated to be 8017.13 J. The semi-cylinder has a curvature that is constant, creating this gradual change in collection values. There are no sharp changes in harvest as displayed in the pi

sinusoidal surface. The smaller rate of curvature on this surface creates a smoother curve at the peak than seen in the pi sinusoid surface. The smoother a curve the easier to track the maximum power point because sharp transitions in the generation are problematic in certain control schemes.

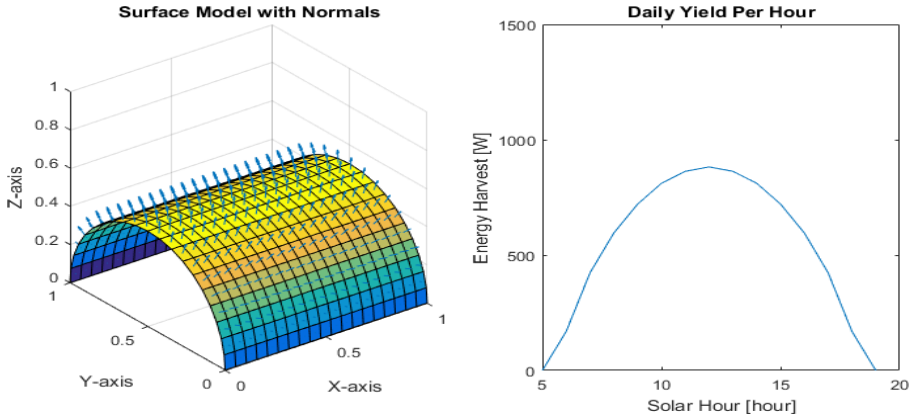

Figure 26: Semi-cylinder model and potential harvest plot

Ellipse Morphology

The ellipse in figure 27 is the similar to the pi sinusoid in that it shows multiple peaks, but due to the surface characteristics at solar noon the light either does not strike the bottom cells or the view factor is too small to make an effect on harvest. The elongated sides allow for the power peaking at 10AM and 3PM with 932.898 W/pu^2. The ellipse benefits from the multiple peaks and since the rate of curvature is less than the pi sinusoid it shows a smooth peak. The total harvest seen was calculated to be 10100.20 J.

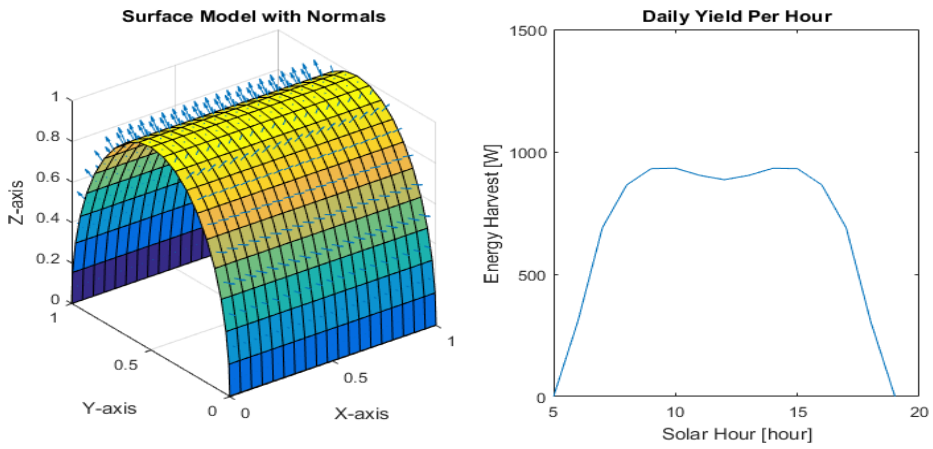

Figure 27: Ellipse model and potential harvest plot

Cone Morphology

The cone surface was selected because of possible practical applications on a curved roof tile. There is still only one axis of curvature, so the requirements of the surface were met. Like the semi-cylinder, there is a gradual rise and fall in the morning and evening. It is clear to see that the peak is significantly smaller than the previous surfaces. The main reason is the smaller footprint needed by the cone. All other figures required the full 1 u^2 surface to collect. The constant curvature creates a peak of 630.6828 W/pu^2 and the reduced footprint results in a total harvest of 5521.8 J.

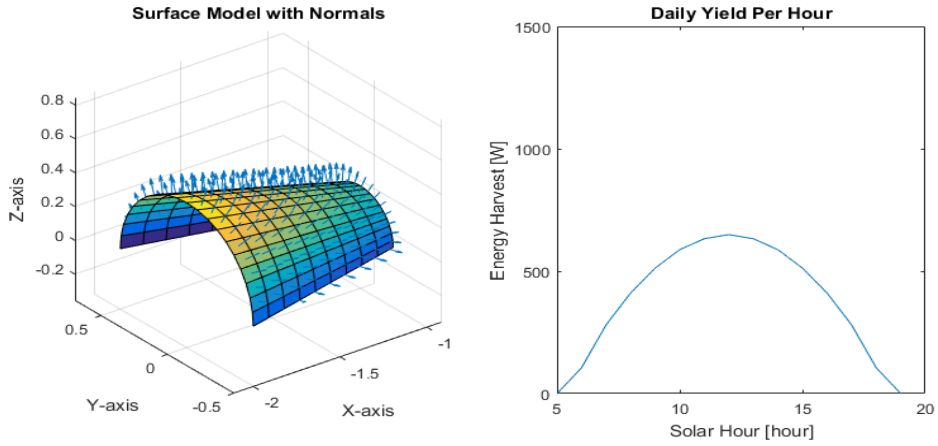

Figure 28: Cone model and potential harvest plot

Comparison of Morphology and Harvest

Two aspect of comparison that were not mentioned were the orientation of the surface and the increase in material area needed for harvest. The orientation depends on specific implementation and desires of the surface, leaving too many variables to consider, so orientation was neglected in the analysis. The surface area however is something to consider when comparing harvest potentials. Table 4 tabulates and orders the surfaces based on surface area. Material area is important when evaluating the production vs cost when implementing solar. The trivial case of the flat plate with a surface area of 1 u^2 will be used to reference how beneficial a nonplanar surface could be. From this analysis, we can see the surface with the largest potential is the ellipse but the surface area is significantly more than most others. The pi/2 sinusoid produces ~9% more energy with respect to the surface area considering the ~3% increase in peak power, given ~14% increase in material needed. This surface produced the largest increase with respect to

actual area of material needed. The least effective surfaces with respect to increased area were the pi sinusoid and the ellipse, excluding the cone since it has a smaller footprint.

Surface	Peak [W]	Total Energy [J]	Surface Area [u^2]
Flat Plate	882.7343	6802.10	1
Pi/2 Sinusoid	960.29	6984.17	1.140
Cone	630.68	5521.80	1.187
Semi-Cylinder	882.98	8017.13	1.569
Pi Sinusoid	890.52	9712.32	2.303
Ellipse	932.90	10100.20	2.420

Table 4: Comparison of potential harvest values

Effect of Cell Geometry on Harvest

Weighting cells with respect to rate of curvature makes sense when addressing the meshing accuracy. Investigation on how the weighting of cells effects the theoretical potential energy harvest. Since the area is a direct factor in determining the harvest capabilities, it stands to reason that adjusting the cell layout would have some effect. The pi/2 sinusoid surface cell layout was used to investigate the effect.

Positive and negative logarithmic weighting schemes were conducted on the surface. Positive weighting reduces the size of the cell widths at higher rates of curvature whereas negative weighting increases the size. Figure 29 displays both the surface structure and the resultant energy harvest plot. The harvest plots are almost identical in energy collected. Figure 30 shows the same surface but with an amplitude of 1 as opposed to 0.5 of the previous.

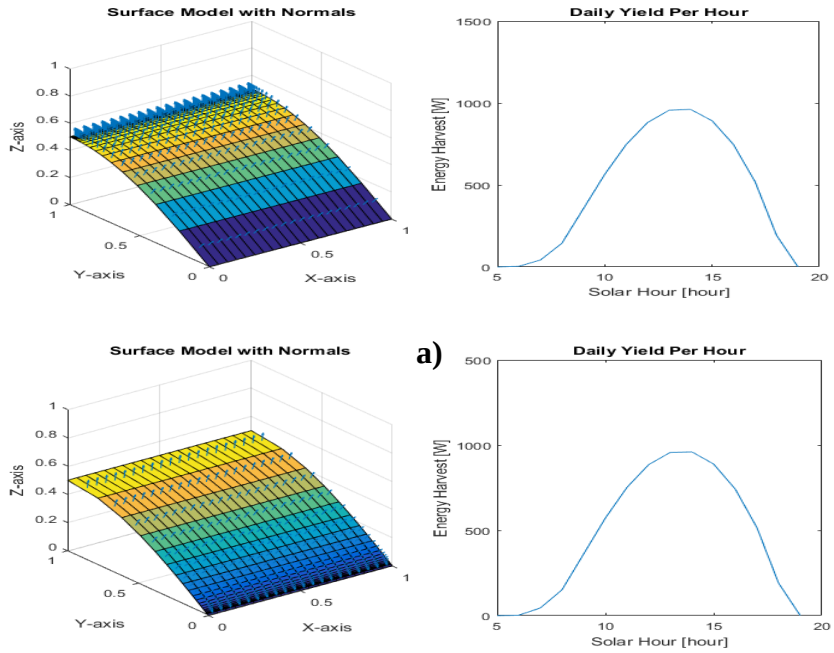

Figure 29: Pi/2 sinusoid model with a b) plitude of 1 and harvest plots for a) positive and b) negative weighted cell structures

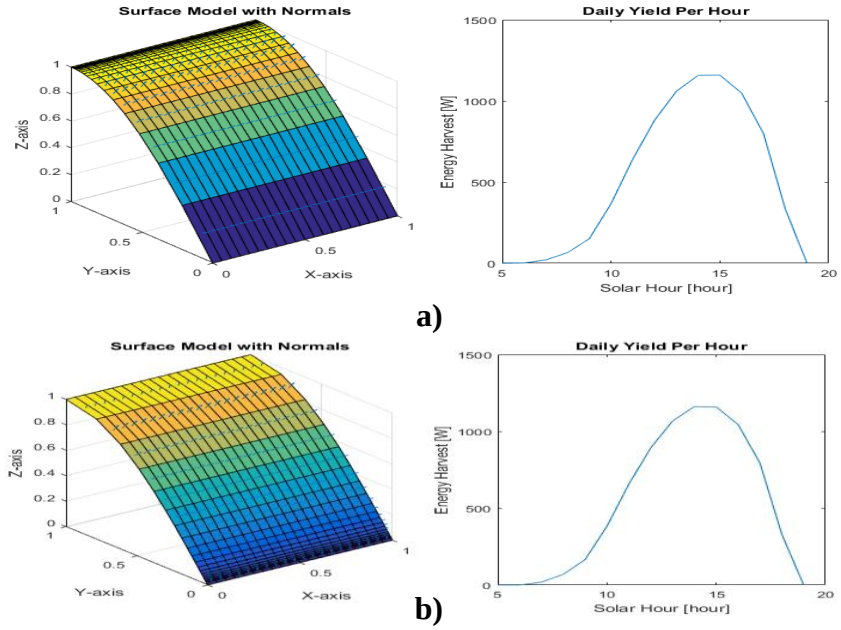

Figure 30: Pi/2 sinusoid model with an amplitude of 1 and harvest plots for a) positive and b) negative weighted cell structures

A closer look into the effects of weighting of the widths of the cells needed to be taken since not much was visibly different from plotting. Table 5 lists the evaluation of the pi/2 sinusoid with respect to three different amplitudes. The non-weighted surface at these amplitudes were also included as references. The single '*' denotes a positive weighting. Alternatively, the double '**' represents negatively weighted. For the 0.5 Amplitude surface the peak power to be approximately the same with very small increase in the positively weighted mesh, but total energy potential was increased by the negatively weighted mesh. This is due to the larger cells near the top receiving insolation at reduced atmospheres, basically harvesting mid-day direct insolation. As the sun sets the air mass ratio increases, effectively reducing the insolation available for collection by the lower cells. For 0.75 amplitude, we see a similar effect where the negatively weighted mesh produces more overall energy, but now it retains a higher peak power as well. We also see a decrease in total energy with the use of positively weighted cells. For 1.00 amplitude, we see a similar trend to that of 0.75. With the increase of surface area from the higher amplitude we collect significantly more energy with still similar peak powers attained.

Surface	Peak Power [W]	Total Energy [J]	Surface Area [u^2]	Amplitude
Sinusoid – pi/2	960.316	7007.388	1.140	0.5
***Sinusoid – pi/2**	960.751	7002.508	1.139	0.5
****Sinusoid – pi/2**	960.357	7025.973	1.140	0.5
Sinusoid –pi/2	1059.031	7299.639	1.287	0.75
***Sinusoid – pi/2**	1059.252	7291.141	1.287	0.75
****Sinusoid – pi/2**	1060.747	7328.914	1.286	0.75
Sinusoid – pi/2	1158.200	7696.873	1.464	1
***Sinusoid – pi/2**	1158.963	7686.023	1.463	1
****Sinusoid – pi/2**	1161.591	7742.532	1.461	1

Table 5: Comparison of harvest values with respect to cell weighting and amplitude of the pi/2 sinusoid

The weighting of the surface showed that the negatively weighted cell structure produces more energy than the positive and non-weighted structures in most of the cases. This increase in harvest based only on the layout of the cells on a surface is specific only to this specific shape. Harvest is highly dependent on the specific surface such that on an ellipse the weighting structure might benefit from a positive weighted cell structure. Weighting the cells on this surface expresses that there is an effect associated with how a surface is partitioned into cells.

Summary of Chapter IV

Chapter IV validates the morphology and provides analysis on the results found. The cell area calculations were validated by comparing their sum with the expected result of 1u^2. Using the flat plate, the view factors were validated by calculating the position of the sun and individual cell normal. The individual cell approach was verified by the summation of individual cell collection with the global harvest expected. Various surfaces were analyzed for potential harvest, finding the ellipse to have the largest potential harvest and the pi/2 sinusoid having the largest increase with respect to increase in material area needed. An investigation on the effect of weighted cell layouts was also conducted, verifying there is an effect to be conscious of.

CHAPTER V

RESULTS OF PIXELIZATION

Pixelization means to group homogeneous or similar enough cells in order to determine an appropriate series connected array. The k-means algorithm is used to cluster cells with similar maximum power points. The semi-cylinder and pi/2 sinusoid surfaces were used to validate this portion of the approach. At each solar positions the maximum power point currents were evaluated and cells were placed in pixels. The number of pixels corresponds to the number of converters required. Since minimizing converters is of high priority, the number of clusters k-means was instructed to create was restricted to five. The following chapter gives the results and analysis of the process selected to reduce the mismatch expected with nonplanar thin film photovoltaics.

Flat Plate Pixelization

The pixelization of a flat plate is the trivial case, but it gives insight to the arbitrary initialization associated with the k-means algorithm. When the flat plate is put through the algorithm, although all cells are homogeneous, there are four single cell pixels shown in figure 31. Each plotted point represents the current output of a cell. This result was expected since k-means is directed to generate a set number of clusters. This trivial analysis gives insight into how the algorithm arbitrarily selects the initial cluster representatives, keeping consistent for every iteration. The homogeneity of the cells on a flat plate was also validated by these results, generating identical current characteristics.

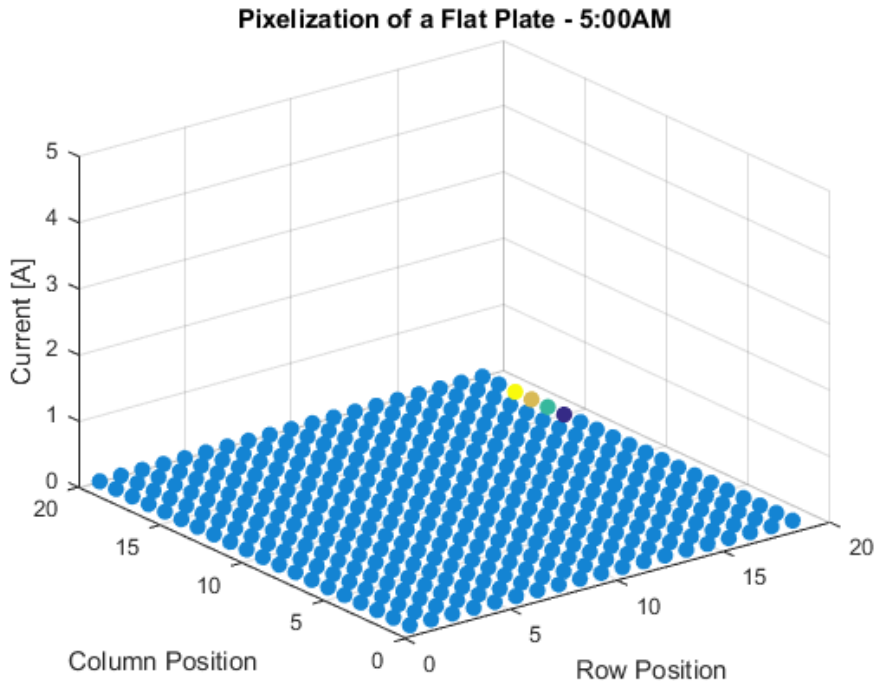

a)

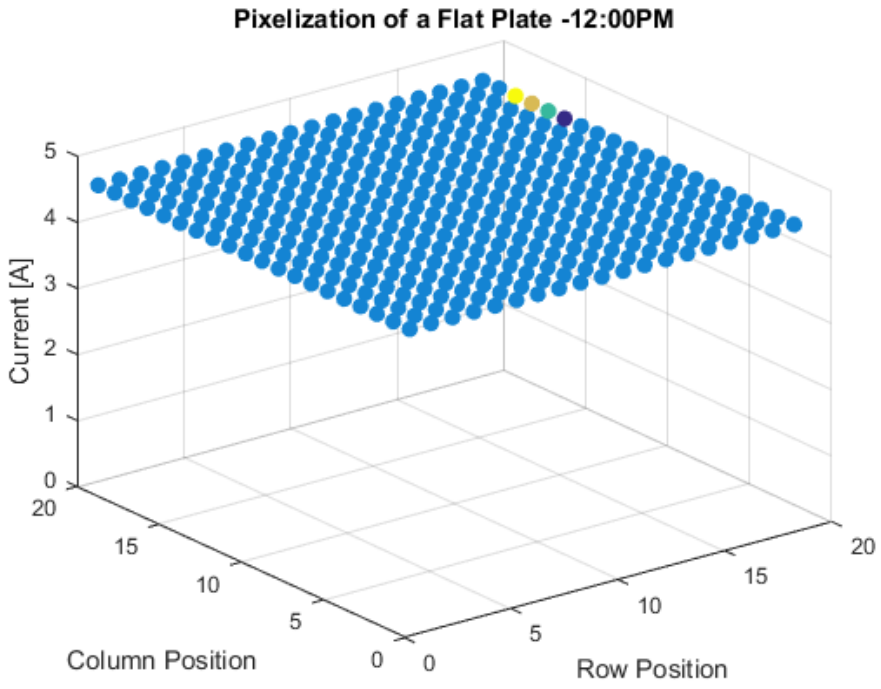

b)

Figure 31: Pixelization of a flat plate at a) 5:00AM and b) 12:00PM

Semi-Cylinder Pixelization

With the introduction of a nonplanar surface the pixelization produces varying results. It is first necessary to understand the indexing method to track the data of individual cells. Figure 32 displays the convention used. Each point on the plot represents a current value produced by the associated cell given by the convention. Each color represents a different pixel generated.

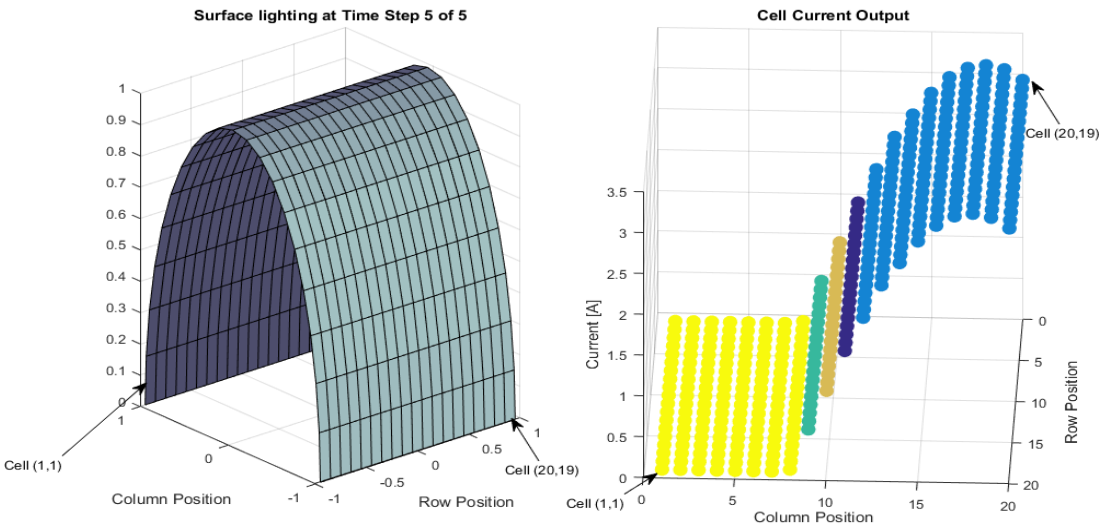

Figure 32: Orientation of the pixelization method used

Pixelization every hour

The trivial method of approach is to generate a new pixel layout for every solar position simulated. This method performed well in minimizing the current mismatch within each pixel. Figure 33 shows the pixelization of the cells at a few associated hourly solar positions. Visual analysis of the pixilation validates this method of approach, but

with current technologies this would be impractical and require complex switching topologies to adjust the interconnections on the surface many times during the day. To minimize the interconnections needed, the method was adjusted to better optimize the system.

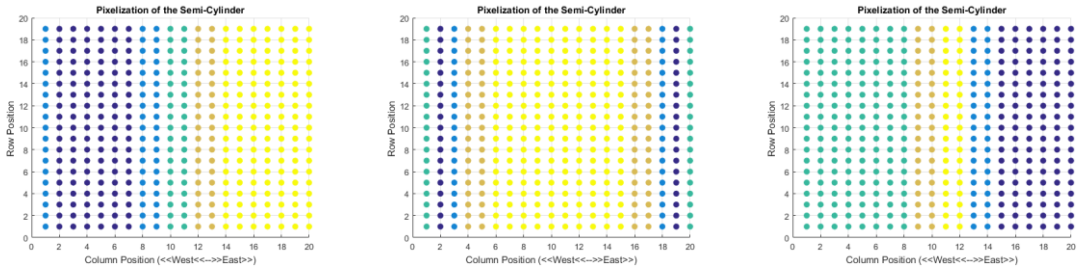

a) 8:00AM b) 12:00PM c) 5:00PM

Figure 33 Pixelization interconnections for 3 of 15 solar positions in the given day

Global pixelization

The next method of approach was to pixelate at every sun position specified and take the most common pixel each cell was clustered into over the course of the day. The application of this would require only five converters to condition this circuit, assuming minimal variance within each pixel. Theoretically this should provide the most appropriate interconnection. Figure 34 displays the most appropriate cell layout for the semi-cylinder. The most notable feature of this layout are the cells on opposite sides of the semi-cylinder are proposed to be an optimal connection. This stems from the symmetric nature of the surface. The variation of the current in a pixel with this attribute would be significant in

both the morning and the evening. Figure 35 shows cells at that generate significant current at 7AM in the morning are designed to connect with cells that produce no current. This cannot be appropriate because when the sun is hitting one side of the semi-cylinder the opposite side will block the generated current if series connected. This brought to light an issue that is specific to surfaces that have curved peaks. Further investigation into the surface is needed in order to minimize this error.

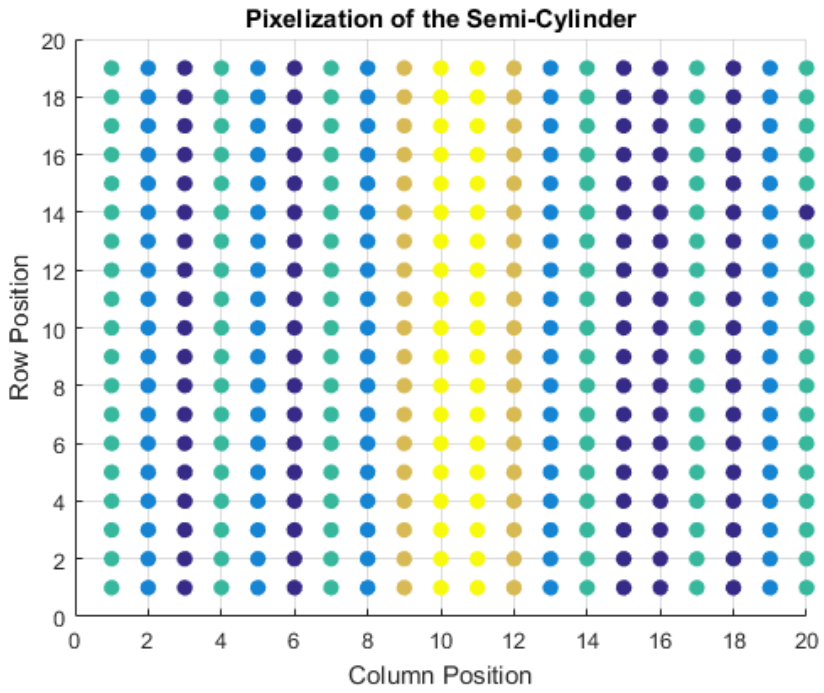

Figure 34: Pixelization interconnection proposed for the semi-cylinder

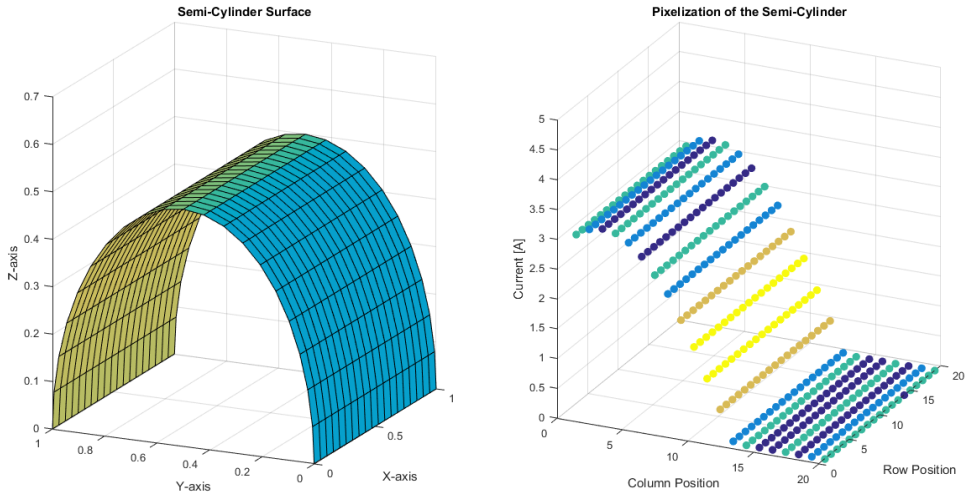

Figure 35: Pixelization interconnection of a semi-cylinder with current variances for an arbitrarily selected solar position

Ranged pixelization

A method to mitigate this error was to divide this analysis into 3 time ranges. Morning, mid-day, and evening ranges were selected to more appropriately minimize current variance by considering the east, west, and overhead positions of the sun. This process developed three distinct interconnection layouts displayed in figure 36. Figure 37 shows the current distribution within each pixelization range. The top, middle, and bottom rows of plots correspond to the morning, mid-day, and evening time ranges, respectively. The first and last pixelizations were omitted due to lack of radiation striking the surface of the cells. Breaking the pixelization into ranges better mitigated the variance of the currents in each pixel or at least better than that of the global pixelization layout.

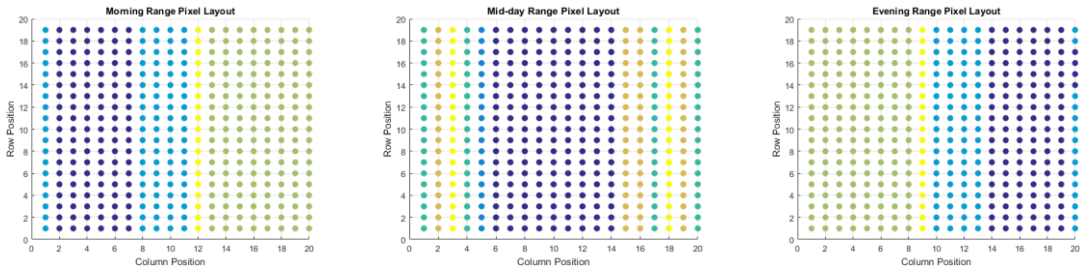

a) Morning Range **b) Mid-day Range** **c) Evening Range**

Figure 36: Pixelization interconnections for 3 distinct ranges of solar positions

There are still problematic clustering errors seen associated with the curvature of the surface once again. Although it is not necessary for adjacent columns of cells be similarly producing, during mid-day hours there are still pixels where some are producing current while others have yet to collect radiation. Meaning, when panels peak at solar noon there will be significant fluctuations and losses when the mismatch due to self-shading is present, although smaller than the global pixelization. Some maximum power point tracking systems struggle with rapid variations, so this is a topic regarding the ability of the power electronics rather than the validation of the pixelization. Since the formulation of much of the error was generated by the characteristics of the semi-cylinder's bidirectional convex structure, analysis of the unidirectional convex structure of the pi/2 sinusoid surface was addressed to see if similar complications appear.

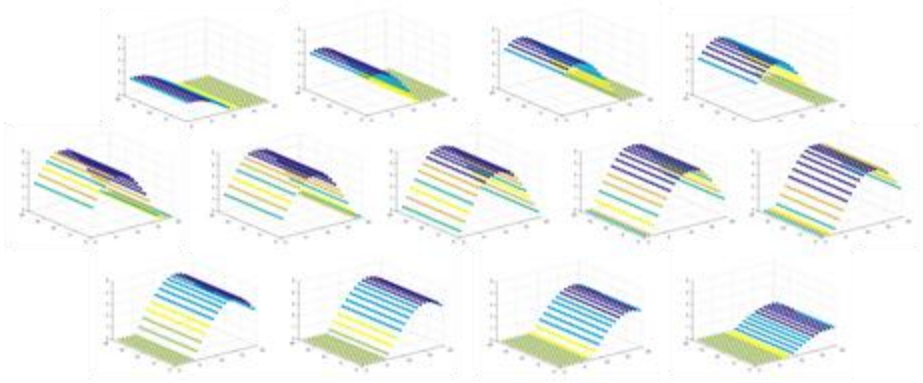

Figure 37: Current distributions within each range of pixelization

Pi/2 Sinusoid Pixelization

Ranged pixelization proved to be the best balance between number of interconnections and current mismatch mitigation, so the pi/2 sinusoid was analyzed under the same method of approach. Within the analysis each pixel is run through several performance indices in order to test the statistical differences apparent after clustering and qualify the method.

Morning range

In the morning range, due to the orientation of the surface when the sun rises in the east the surface will see hardly any insolation. The arbitrarily selected solar position at 7:00AM was selected for analysis. Figure 38 shows the shaded surface and the pixelization layout. The pixelization of this range provided only one active pixel. It is evident that at this specific solar position this interconnection is valid. This may or may not be representative of all the solar positions within this range, but it serves to prove that there is validity in the process. Table 6 breaks down the current values and the associated

performance indices used. As stated before, pixel 5 was the only active pixel for this solar position and it performed perfectly with respect to collecting similar producing cells. There was no variance in current produced so the most accurate cluster expected. The '*' denotes null or inappropriate pixels. The largest pixel contained 377 of the cells, but due to this there was some variance in produced current, ranging from 0.7A in one row of cells to 0A in the rest of the pixel. This large cell is evident of the sunlight being unable to reach the face of the cells in the early morning hours, so the clustered cells produced 0A for most this range. Large pixels like this can be problematic if there are rapid changes in insolation seen by the surface. It being a larger area there are instances where one side of the pixel is producing higher than the other. Although it seems to be appropriate for this specific case, a more equal distribution of cells per pixel is beneficial to the overall system. All things considered, the pixelization did well to cluster similar cells with respect to the 7:00AM solar position despite the lack of insolation striking the surface.

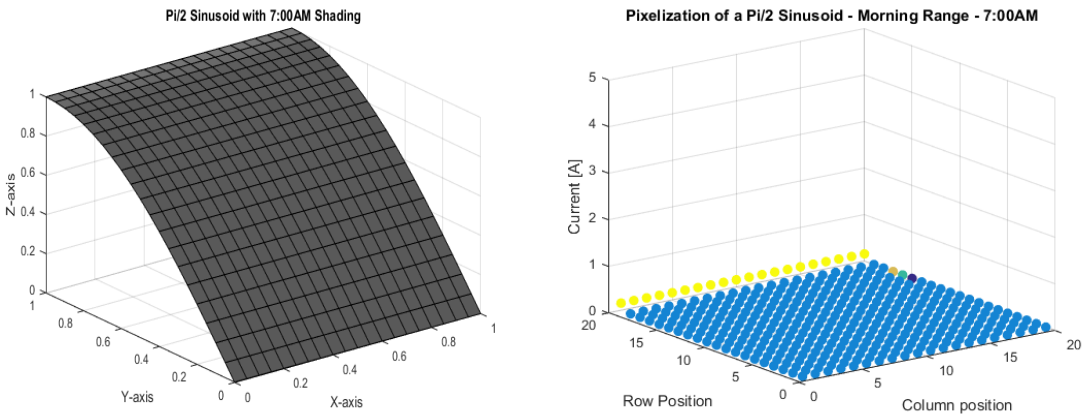

Figure 38: Surface and morning range pixelization layout of the pi/2 sinusoid

Solar Time	Pixel	# of Cells	Variance [A]	Standard Deviation [A]	Max [A]	Min [A]	Range [A]
8:00 AM	1*	1	-	-	0	0	0
8:00 AM	2*	377	0.0300	0.1732	0.7088	0	0.7088
8:00 AM	3*	1	-	-	0	0	0
8:00 AM	4*	1	-	-	0	0	0
8:00 AM	5	20	0	0	1.0804	1.0804	0

Table 6: Analysis of morning range pixelization on the pi/2 sinusoid

Mid-day range

This pixelization layout performed better in comparison to the morning range solely because there was more insolation therefore more data for the clustering algorithm to iterate through. The arbitrary solar position was selected to be 11:00AM for the analysis of the pixelization. Figure 39 displays the shaded surface at 11:00 AM and the pixelization layout once again. At first glance the yellow cells, pixel 5, shows the most visible variance due to the curvature of the surface. A statistical analysis was done to verify further. Before mentioning the analysis, notice in Table 7 the number of pixels is more distributed within this time range. There are still somewhat large pixels, but is far more appropriate than before. Pixel 4 was the best performing pixel out of the five. The range only reached 0.17A and the variance and standard deviation were relatively small values at 0.007A and 0.86A

respectively. Pixels 2 and 3 also performed well at this hour. For pixels 1 and 5 there are again larger clusters generated, resulting in large ranges and significantly large statistical indices. The large ranges of these two pixels is largely attributed to the rapid change of the view factors on the surface due to the relative quickness of the sun during these hours. Referring to figure 38, the rapid increase is visible on the pixelization layout. Much like the sun path across the sky, at a distance a speeding car seems to be slow and as it gets closer the observer sees the car move faster. Since the sun is the closest to the earth at solar noon, it is effectively seen as moving faster across the sky. This movement of the sun results in the cell's current to fluctuate more rapidly in this range of time. Another issue seen is the overlapping of the current ranges between the pixels. This could be another effect of the sun or surface characteristics, but it is more likely that the arbitrary initialization is to blame for this. If k-means selects arbitrary pixels in relative proximity it is intuitive that they will overlap. This can be rectified with the use of alternate algorithms with more appropriate initialization methods.

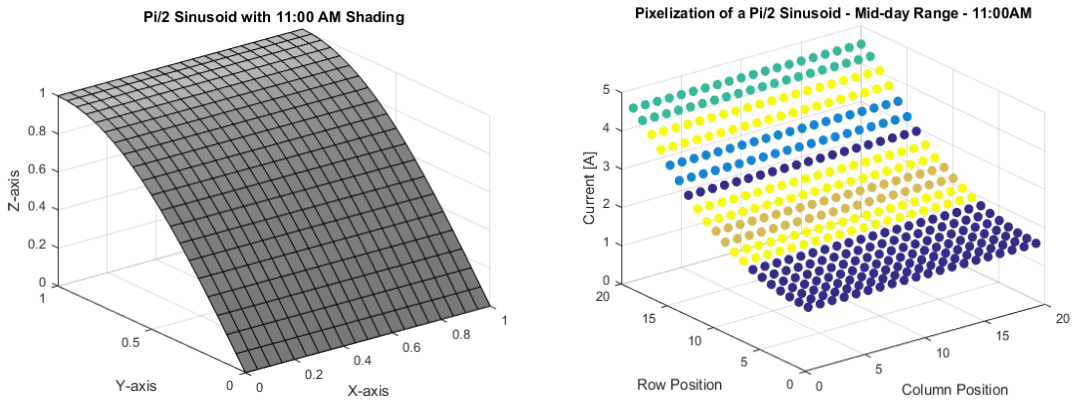

Figure 39: Surface and mid-day range pixelization layout of the pi/2 sinusoid

Solar Time	Pixel	# of Cells	Variance [A]	Standard Deviation [A]	Max [A]	Min [A]	Range [A]
11:00 PM	1	160	0.2024	0.4499	2.9148	1.4767	1.4381
11:00 PM	2	40	0.0209	0.1445	3.4681	3.1828	0.2853
11:00 PM	3	40	0.0108	0.1038	4.5023	4.2973	0.2050
11:00 PM	4	40	0.0074	0.0860	2.3184	2.1486	0.1699
11:00 PM	5	120	0.6880	0.8295	4.0430	1.8773	2.1658

Table 7: Analysis of mid-day range pixelization on the pi/2 sinusoid

Evening range

The solar position at 4:00PM was arbitrarily selected to qualify the pixelization layout of the evening hours. This range produced much better results than the previous two. This could be a result of the smooth nature of the currents being generated later in the day as shown on the pixelization plot in figure 40. A smaller fluctuation of current makes it easier for k-means to produce beneficial clusters. The linear nature of the lower end of the surface also reduces the rapid change in view factor that was seen in the mid-day hours at the curved knee of the surface. Referring to table 8 the range is minimized to be less than zero in all pixels. The standard deviation and variation statistical indices remain relatively small with respect to the previous ranges. Even the pixels with 100 and

219 cells were controlled well enough to return incredibly low fluctuations within their respective pixels. Again, this serves to emphasize that large cells are not always inappropriate because it depends on surface characteristics and clustering parameters which is why in the first two ranges it was a negative attribute.

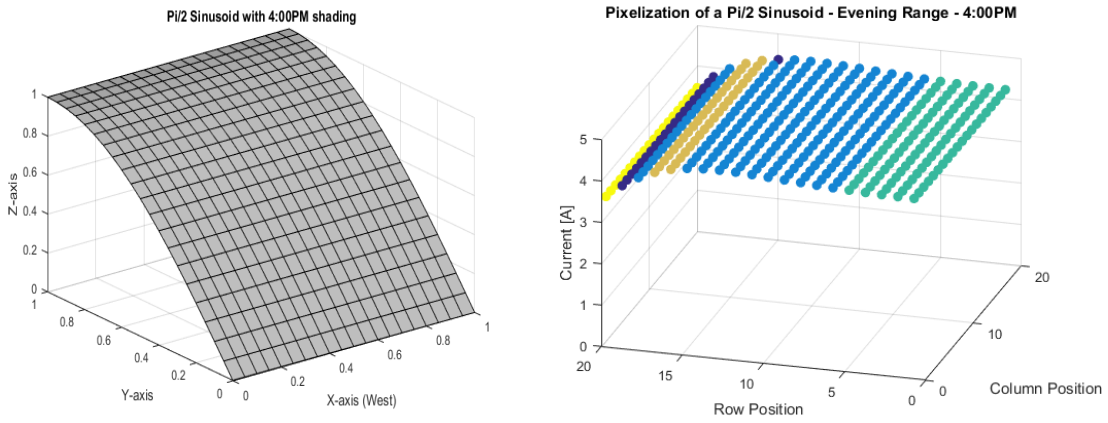

Figure 40: Surface and evening range pixelization layout of the pi/2 sinusoid

Time Step	Pixel	# of Cells	Variance [A]	Standard Deviation [A]	Max [A]	Min [A]	Range [A]
4:00 PM	1	21	0.0359	0.1895	3.7521	2.8838	0.8684
4:00 PM	2	219	0.0548	0.2340	4.0150	3.1894	0.8256
4:00 PM	3	100	0	0.0022	4.0124	4.0062	0.0062
4:00 PM	4	40	0.0087	0.0935	3.6171	3.4324	0.1847
4:00 PM	5	20	0	0	2.5192	2.5192	0

Table 8: Analysis of evening range pixelization on the pi/2 sinusoid

Summary of Chapter V

This chapter gives insight into how well a data clustering algorithm, k-means, can perform when implemented to cluster homogeneously producing cells. After qualifying this this method, several statements can be confidently made. K-means performed well in clustering cells on surfaces that have lower rates of curvature, since in the mid-day range error was caused by the rapidly changing view factor around the knee or peak of the surface. There is also reason to believe the arbitrary initialization of this algorithm causes the overlap of current ranges within each pixel. Implementing an algorithm that allows for non-arbitrary starting points could benefit the output of this approach. Overall, the method using a clustering algorithm has potential to further improve the likelihood of practical thin film photovoltaic systems.

CHAPTER VI

SUMMARY AND CONCLUSIONS

Advancements in PV technologies have surpassed the need to be rigid and flat previously required by conventional crystalline silicon solar cells. This thesis presents a mathematical tool capable of modeling and analyzing the added complexities of nonplanar PV. This tool can determine the impact that curved geometries have on the potential harvest by way of individual cell analysis and reduce current density variance with the use of the k-means clustering method.

Morphology

Using the proposed approach, the model is able to determine the gradient of view factors on a non-flat surface for further study. The characteristics of the surfaces were modelled by way of a rectangular meshing structure for accurate approximation of the varying view factors that appear on arbitrary nonplanar surfaces. In the first analysis, the results show that when compared to the flat panel a curved surface will produce more in the equivalent footprint of area. Comparison between different curved surfaces was also presented to show how different surface characteristics can affect the energy harvest plot of any given day, neglecting changes in orientation. Also included was an analysis of power increased with respect to area since material cost is of importance in any feasibility study. Also, an investigation on how the geometrical layout of the mesh affects the harvest was also done. By adjusting the widths logarithmically, either positively or negatively, the

model concluded that there is a slight change based on geometry alone. Although geometrical mesh weighting was not that significant for total harvest potential, it could be beneficial for the mitigation of mismatch current attempted by the pixelization method in the proposed approach by possibly reducing the current swings caused by the curves of surfaces at the peak.

Pixelization

The model was able to verify approximate view factor gradients across a curved surface, and with the implementation of an electrical model the current mismatch of the cells can be studied as well. When solar cells are series connected, it needs to have equivalent current, otherwise circulating current will create losses leading to hot spots and degradation of the material. This is a result consistent with shading on a conventional crystalline solar cell. Non-homogeneously producing cells are a major hurdle for flexible thin film PV because it is not just caused by shading but also inherent in the characteristics of the surface. This thesis proposed a method of approach called pixelization which utilizes the k-means clustering algorithm to mitigate this variance of current in series connected groups of cells, otherwise known as pixels. The method proved to have significance in grouping pixels on a unidirectional surface rather than a bidirectional surface. Upon further investigation, the method was adjusted to account for the rise and fall of a bidirectional surface, producing lower variations within each pixel. Lastly, a numerical analysis of the k-means clustering was presented on a unidirectional curved surface resulting in even more of a reduction of variance and range within each pixel. The

approach using a mathematical clustering algorithm benefited the goal of reducing current mismatch of a nonplanar system while providing insight on how to improve even further with this knowledge.

Potential Future Work

The work presented in this thesis is merely a base for the study of nonplanar photovoltaics modelling. Now that the structure has been formulated and showed valid results there are aspects of this approach that require integration for a more accurate and practical model. In the morphology method of the approach the implementation of alternate meshing structures could improve the accuracy and precision of the characteristic data of the surfaces. Adjusting the computations for approximation of the view factor associated with each cell would also greatly benefit the model if done with respect to the rate of curvature seen on the face of the cell. Since the computation of the surface parameters were based off 1-DOF figures, a change of equations should be done to address surfaces like a hemisphere or wavy surface.

With respect to the electrical computations done there is room to develop. Adding more accurate models like the TDM would be beneficial for the accuracy of the generated output current of the model. An effect that is not considered with the various models of solar cells is the thermal gradient. Like that of the view factor, the temperature is also a gradient since thermal radiation is the basis for view factor in the first place. Also, a better understanding of the apparent temperature gradient as the sun crosses the sky will be a

defining factor of the efficiency of a practical model. Figure 41 shows the thermal gradient present on curved roof tiles that validate this statement.

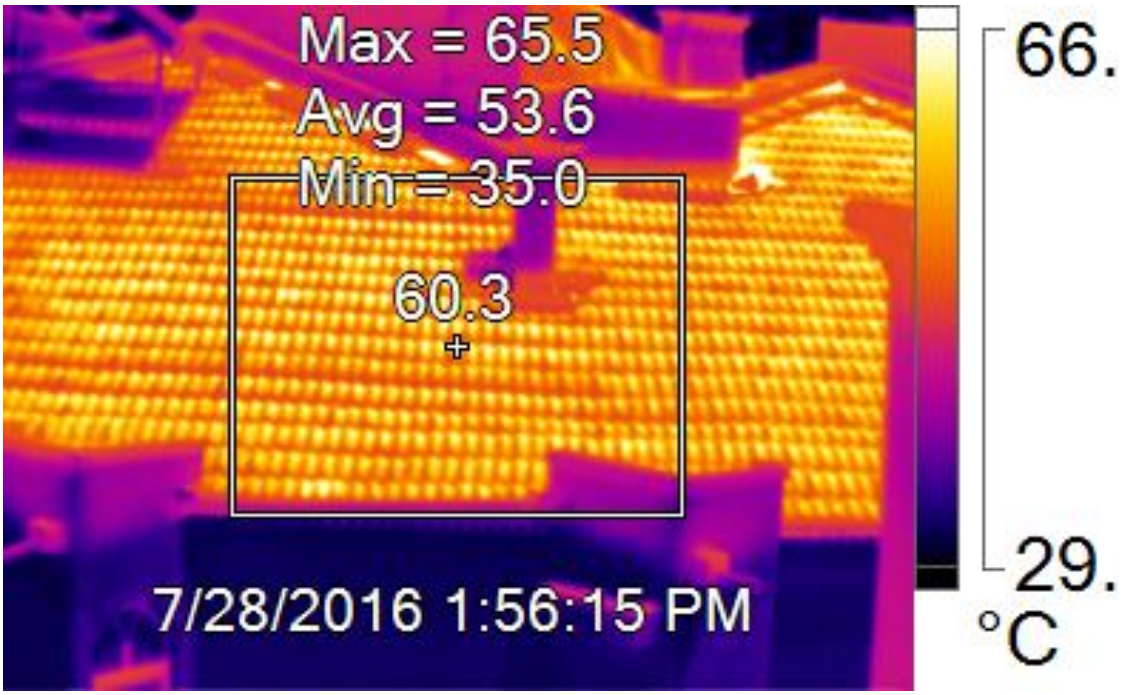

Figure 41: Thermal gradient of curved roof tiles

Future work with the pixelization method determining the best method for determining appropriate series connected cells has a variety of directions for improvement. The structure of the k-means algorithm was restricted by the number of pixels to generate by the user. Using an algorithm that would produce an appropriate number of clusters for actual maximum efficiency of the computation would benefit this approach. Another aspect of the pixelization method that would benefit from a different algorithm would be the arbitrary selection of cluster representatives initialized by k-means. This created an

overlap of the current ranges within each pixel, increasing the variance. There is a plethora of mathematical clustering techniques for possible implementation that only need to be introduced to make a difference in this work.

Including the $i - v$ characteristics of the array after the series interconnections are determined would also increase the impact of this work. The series connected arrays from the pixelization method will still have some variance in currents, but ideally at a reduced amount. The ability to compute the resultant power delivered and power loses in the solar system would benefit further analysis. With the addition of this process there would be a comprehensive model to compare an experimental output to. Because of the losses in the system and the effects of the minor current variance left there will be evident attenuations such that the output will not meet the potential harvest plots presented. This approach could serve as an asset in feasibility studies of various PV energy generation systems with an accurate analysis of all major factors.

Final Thoughts

This thesis provides a tool in the form of a modeling approach for nonplanar thin film PV systems. This work was not done to provide a final analysis to determine the best parameters of a nonplanar solar panel. There are many variables that are not determined like how pixel switching can be achieved, how orientation affects various surfaces, or what the desired performance is. The last two are completely dependent on application specifics. For example, a system requiring starting power for a motor in the morning can be adjusted for that specific purpose by shifting azimuth and tilt east. Alternatively, for a

system that requires peaks both in the morning and evening it would require different orientation. Overall this tool provides information on flexible thin film that was previously unknown, and with continued research could be a valuable asset to have in the near future.

REFERENCES

[1] I. E. Agency. (2016), Key Renewables Trends. *Renewables information*. Available: www.eia.org

[2] D. C. F. Power. (2015), US Solar Power Growth through 2040 Exponential or inconsequintial? Available: http://www2.deloitte.com/content/dam/Deloitte/us/Documents/energy-resources/us-er-solar-innovation-growth.pdf

[3] N. R. E. Laboratory. (2016). *Photovoltaic Research*. Available: http://www.nrel.gov/pv/assets/images/efficiency_chart.jpg

[4] Y. Hamakawa. "Thin-Film Solar Cells," *Springer Series in Photovoltaics*, vol. 13: Springer Belin Heidelberg, 2004.

[5] T. Söderström, F.-J. Haug, V. Terrazzoni-Daudrix, and C. Ballif, "Optimization of amorphous silicon thin film solar cells for flexible photovoltaics," *Journal of Applied Physics*, vol. 103, p. 114509, 2008.

[6] M. A. Green, "Third Generation Photovoltaics," *Springer Series in Photovoltaics*, vol. 12: Springer Berlin Heidelberg, 2003.

[7] C. Y. Peng, S. Lu, T. P. Dhakal, C. R. Westgate, S. Garner, and P. Cimo, "Fabrication of Cu2ZnSnS4 solar cell on a flexible glass substrate," *Thin Solid Films*, vol. 562, pp. 574-577, July 2014.

[8] A. Salavei, D. Menossi, F. Piccinelli, A. Kumar, G. Mariotto, M. Barbato, *et al.*, "Comparison of high efficiency flexible CdTe solar cells on different substrates at low temperature deposition," *Solar Energy*, vol. 139, pp. 13-18, December 2016.

[9] M. Bojic, J. Radulovic, V. Rankovic, D. Nikolic, L. Bojic, and J. Skerlic, "FLEXIBLE THIN-FILM SOLAR PHOTOVOLTAICS: RESEARCH AND APPLICATION," *Annals of the Faculty of Engineering Hunedoara - International Journal of Engineering,* vol. 14, pp. 37-40, 2016.

[10] F. C. Krebs, T. Tromholt, and M. Jorgensen, "Upscaling of polymer solar cell fabrication using full roll-to-roll processing," *Nanoscale,* vol. 2, pp. 873-886, 2010.

[11] M. S. C. S. Y. C. Lee, Y. L. Lin, B. G. Mason, E. A. Novakovskaia, and V. R. Connell, "Integrated Flexible Solar Cell Material and Method of Production," U.S. Patent 6,224,016, 2001.

[12] J. Gazda, "Weavable fiber photovoltaic collectors," ed: Google Patents, 2009.

[13] N. G. Dhere, A. Kaul, S. A. Pethe, E. Schneller, and N. S. Shiradkar, "Outdoor performance testing of thin-film PV modules in the hot and humid climate," in *2013 IEEE 39th Photovoltaic Specialists Conference (PVSC)*, 2013, pp. 2994-2997.

[14] S. R. Athreya, R. Sharma, K. Kauffmann, L. L, x00F, pez, *et al.*, "Simulation guided design of flexible photovoltaic laminates," in *Photovoltaic Specialists Conference (PVSC), 2012 38th IEEE*, 2012, pp. 001952-001957.

[15] J. Liang, J. Gong, J. Zhou, A. N. Ibrahim, and M. Li, "An open-source 3D solar radiation model integrated with a 3D Geographic Information System," *Environmental Modelling & Software,* vol. 64, pp. 94-101, 2015.

[16] F. Díaz, G. Montero, J. M. Escobar, E. Rodríguez, and R. Montenegro, "A new predictive solar radiation numerical model," *Applied Mathematics and Computation,* vol. 267, pp. 596-603, September 2015.

[17] D. J. d. y. c. Wojcicki, "Derivation of the effective beam radiation incidence angle equations for diffuse and reflected solar radiation using a two dimensional approach," *Solar Energy,* vol. 112, pp. 272-281, 2015.

[18] H. Li, X. Bu, Z. Long, L. Zhao, and W. Ma, "Calculating the diffuse solar radiation in regions without solar radiation measurements," *Energy*, 2012.

[19] B. Petter Jelle, C. Breivik, and H. Drolsum Røkenes, "Building integrated photovoltaic products: A state-of-the-art review and future research opportunities," *Solar Energy Materials and Solar Cells*, vol. 100, pp. 69-96, 2012.

[20] D. Picault, B. Raison, S. Bacha, J. de la Casa, and J. Aguilera, "Forecasting photovoltaic array power production subject to mismatch losses," *Solar Energy*, vol. 84, pp. 1301-1309, July 2010.

[21] M. B. Shadmand and R. S. Balog, "Mitigating variability of high penetration photovoltaic systems in a community smart microgrid using non-flat photovoltaic modules," in *2013 IEEE Energy Conversion Congress and Exposition*, 2013, pp. 554-560.

[22] M. B. Shadmand and R. S. Balog, "Design considerations for long-term remote photovoltaic-based power supply using non-planar photovoltaic surfaces," in *Technologies for Homeland Security (HST), 2013 IEEE International Conference on*, 2013, pp. 677-682.

[23] H. Zhang and R. S. Balog, "Experimental verification of energy harvest from non-planar photovoltaic surfaces," in *2013 IEEE Energy Conversion Congress and Exposition*, 2013, pp. 4481-4487.

[24] A. Karavadi, *Power Electronics Design Implications of Novel Photovoltaic Collector Geometries and Their Application for Increased Energy Harvest*, 2011.

[25] H. Hagen, *Topics in surface modeling. edited by Hans Hagen*: Philadelphia : Society for Industrial and Applied Mathematics, [1992], 1992.

[26] A. Groenewolt, J. Bakker, J. Hofer, Z. Nagy, and A. Schlüter, "Methods for modelling and analysis of bendable photovoltaic modules on irregularly curved surfaces," *International Journal of Energy & Environmental Engineering*, vol. 7, p. 261, September 2016.

[27] Y. Mahmoud, W. Xiao, and H. H. Zeineldin, "A simple approach to modeling and simulation of photovoltaic modules," *IEEE Transactions on Sustainable Energy,* vol. 3, pp. 185-186, 01 / 01 / 2012.

[28] A. Anurag, S. Bal, and S. Sourav, "A Comparative Study of Mathematical Modeling of Photovoltaic Array," *International Journal of Emerging Electric Power Systems,* vol. 15, pp. 313-326, 2014.

[29] M. G. Villalva, J. R. Gazoli, and E. R. Filho, "Comprehensive approach to modeling and simulation of photovoltaic arrays," *IEEE Transactions on Power Electronics,* vol. 24, pp. 1198-1208, 01 / 01 / 2009.

[30] X. Weidong, W. G. Dunford, and A. Capel, "A novel modeling method for photovoltaic cells," in *Power Electronics Specialists Conference, 2004. PESC 04. 2004 IEEE 35th Annual*, 2004, pp. 1950-1956 Vol.3.

[31] M. Azab, "Improved circuit model of photovoltaic array," *International journal of electrical power and energy systems engineering,* vol. 2, pp. 185-188, 2009.

[32] S. Bal, A. Anurag, M. Nanda, and S. Sourav, "Comprehensive analysis and experimental validation of an improved mathematical modeling of photovoltaic array," *Advances in Power Electronics,* vol. 2015, 01 / 01 / 2015.

[33] A. Bouraiou, M. Hamouda, A. Chaker, M. Sadok, M. Mostefaoui, and S. Lachtar, "Modeling and Simulation of Photovoltaic Module and Array Based on One and Two Diode Model Using Matlab/Simulink," *Energy Procedia*, vol. 74, pp. 864-877, 2015/08/01 2015.

[34] R. W. Andrews, A. Pollard, and J. M. Pearce, "Improved parametric empirical determination of module short circuit current for modelling and optimization of solar photovoltaic systems," *Solar Energy,* vol. 86, pp. 2240-2254, September 2012.

[35] R. Miceli, A. Orioli, and A. Di Gangi, "A procedure to calculate the I–V characteristics of thin-film photovoltaic modules using an explicit rational form," *Applied Energy,* vol. 155, pp. 613-628, 10/1/ 2015.

[36] M. S. Ismail, M. Moghavvemi, and T. M. I. Mahlia, "Characterization of PV panel and global optimization of its model parameters using genetic algorithm," *Energy Conversion and Management,* vol. 73, pp. 10-25, September 2013.

[37] W. De Soto, S. A. Klein, and W. A. Beckman, "Improvement and validation of a model for photovoltaic array performance," *Solar Energy,* vol. 80, pp. 78-88, January 2006.

[38] A. Dolara, S. Leva, and G. Manzolini, "Comparison of different physical models for PV power output prediction," *Solar Energy,* vol. 119, pp. 83-99, September 2015.

[39] X. Yuan, Y. Xiang, and Y. He, "Parameter extraction of solar cell models using mutative-scale parallel chaos optimization algorithm," *Solar Energy,* vol. 108, pp. 238-251, October 2014.

[40] B. E. Pieters and U. Rau, "A new 2D model for the electrical potential in a cell stripe in thin-film solar modules including local defects," *Progress in Photovoltaics: Research and Applications,* vol. 23, pp. 331-339, 2015.

[41] A. Reza Reisi, M. Hassan Moradi, and S. Jamasb, "Classification and comparison of maximum power point tracking techniques for photovoltaic system: A review," *Renewable and Sustainable Energy Reviews,* vol. 19, pp. 433-443, March 2013.

[42] N. Femia, G. Petrone, G. Spagnuolo, and M. Vitelli, "Optimization of perturb and observe maximum power point tracking method," *IEEE Transactions on Power Electronics,* vol. 20, pp. 963-973, 2005.

[43] M. Mousa, M. E. Ahmed, and M. Orabi, "New converter circuitry for PV applications using multilevel converters," in *INTELEC 2009-31st International Telecommunications Energy Conference,* 2009, pp. 1-6.

[44] M. B. Shadmand, M. Mosa, R. S. Balog, and H. A. Rub, "Maximum power point tracking of grid connected photovoltaic system employing model predictive

control," in *2015 IEEE Applied Power Electronics Conference and Exposition (APEC)*, 2015, pp. 3067-3074.

[45] A. F. Mills, *Heat transfer. 2nd ed. A.F. Mills*: Upper Saddle River, N.J. : Prentice Hall, [1999]. 2nd ed., 1999.

[46] T. Maor and J. Appelbaum, "View factors of photovoltaic collector systems," *Solar Energy,* vol. 86, pp. 1701-1708, June 2012.

[47] N. D. Kaushika and A. K. Rai, "An investigation of mismatch losses in solar photovoltaic cell networks," *Energy,* vol. 32, pp. 755-759, May 2007.

[48] G. M. Masters, *Renewable and Efficient Electric Power Systems (2nd Edition)*. Somerset, NJ, USA: John Wiley & Sons, 2013.

[49] B. Andreopoulos, A. An, X. Wang, and M. Schroeder, "A roadmap of clustering algorithms: finding a match for a biomedical application," *Briefings in Bioinformatics,* vol. 10, pp. 297-314, 2009.

[50] H. Li, X. Deng, E. P. Smith, and C. A. Dolloff, "Bivariate functional data clustering: Grouping streams based on a varying coefficient model of the stream water and air temperature relationship," *Environmetrics,* vol. 27, pp. 15-26, 02 / 01 / 2016.

[51] B. F. Solaiman and A. Sheta, "Energy optimization in wireless sensor networks using a hybrid K-means PSO clustering algorithm," *Turkish Journal of Electrical Engineering & Computer Sciences,* vol. 24, pp. 2679-2695, July 2016.

[52] C. C. Aggarwal, C. K. Reddy, *Chapman & Hall/CRC Data Mining and Knowledge Discovery Series : Data Clustering : Algorithms and Applications (1)*. Boca Raton, US: Chapman and Hall/CRC, 2013.

[53] P. N. Tan, M. Steinbach, and V. Kumar, "Data mining cluster analysis: Basic concepts and algorithms," 1st ed. Boston : Pearson Addison Wesley, 2005.

APPENDIX A

Outline of Method

```
clear
close all

%% User Interface - Parameter Selection
numPix = 5; % Desired # of switching configurations
n = 173;
Lat = 23.45;
Lon = 0;
phi = 0;
tilt = 0;

%% Non User Interface - Parameter Selection
Surface = 'Flat Plate'
% Surface = 'SemiCylinder'
% Surface = 'Cone';
% Surface = 'Sinusoidal - pi'
% Surface = 'Sinusoidal - pi/2'
% Surface = 'Ellipsoid'

% declination angle
d = 23.45*sind((360/365)*(n-81));



%% Generate Surface
% Input: phi, tilt
% Output:[x,y,z]
[x,y,z] = SurfaceGeneration(Surface,phi,tilt);
figure()
surf(x,y,z)
title(strcat(Surface,' Surface'))
ylabel('Y-axis (North)')
xlabel('X-axis (West)')
zlabel('Z-axis')


%% Find Cell Face Components
% Output: Area, Center, Normal
[Area,Center,Normal] = Face(x,y,z);

% indexing for faces, edges, and vertices
[vertices,faces] = surfToMesh(x,y,z);edges = meshEdges(faces);
    nU = Normal(:,:,1); nV = Normal(:,:,2); nW = Normal(:,:,3);
    nX = Center(:,:,1); nY = Center(:,:,2); nZ = Center(:,:,3);

%% Calculate Time Parameters
[Rise,Set] = Daylight(Lat,Lon,d);
```

```
%% Select number of evaluations
StepSize = -1;
TimeSteps = numel(Rise:StepSize:Set);


%% Determine Solar Position & Magnitude of Radiation
% A & k are fitted curves for a specific example in Masters
% Extraterrestrial Flux (radiation)
A = 1160 + (75*sind((360/365)*(n-275)));
% Optical Depth
k = 0.174+ (0.035*sind((360/365)*(n-100)));
run('SunFluxPosition');


%% Individual Cell Approach (Cell Scope)
% % Calculates the View Factor(VF) or Angle of Incidence of each cell
face
% % Computes the Insolation seen by each cell at each iterated time
% % step
[BeamIn, TotalEnergy, EnergyPerHour, Gb,Incidence, InstaEnergy,VF] =
Insolation;
figure()
plot(Rise:-1:Set,EnergyPerHour)


%% Electrical calculations
% range of voltage outputs
Va = 0:0.01:1.5;
% Collector temperature
Tc = 25;
% Initializing variables
I = cell(size(Area,1),size(Area,2),TimeSteps);
P = cell(size(Area,1),size(Area,2),TimeSteps);
MPP = cell(size(Area,1),size(Area,2),TimeSteps);
Vmpp = zeros(size(Area,1),size(Area,2),TimeSteps);
Impp = zeros(size(Area,1),size(Area,2),TimeSteps);

for kdx = 1:1:TimeSteps
    for idx = 1:size(Area,1)
        for jdx = 1:size(Area,2)
            % Current characteristics
            I{idx,jdx,kdx} = ISDMcurves(Va,Gb(idx,jdx,kdx),Tc);
            % Extract power data
            P{idx,jdx,kdx}(1,:) = Va.*I{idx,jdx,kdx};
                  index =
                  find(P{idx,jdx,kdx}(1,:)==max(P{idx,jdx,kdx}(1,:)));
            % Extract maximum power point data
            Vmpp(idx,jdx,kdx) = Va(index);
            Impp(idx,jdx,kdx) = I{idx,jdx,kdx}(index);
            MPP{idx,jdx,kdx} = [Impp(idx,jdx,kdx),Va(index)];
```

```
        end end end

%% Pixelization of Cells

% This creates a single interconnection for all solar positions
% [PixelRef, PixelMap,CCent,Fuzz] = Pixelate(Impp,numPix,TimeSteps);
% [PixelRef, PixelMap] = Pixelate(Impp,numPix,TimeSteps);

% This sections the time steps into 3 interconnection groups
[PixelRef1,PixelRef2,PixelRef3] = Pixelate2(Impp,numPix,TimeSteps);

% This creates a new configuration for every solar position
% [PixelRef, PixelMap] = Pixelate3(Impp,numPix,TimeSteps);

%% Find Surface Area
SurfaceArea = sum(sum(Area),2);

%% Find Peak Power
Peak = max(EnergyPerHour);
```

Surface Generation Function

```
function [x,y,z] = SurfaceGeneration(Surface,phi,tilt)

%% Generate Surface with identical pixel geometry and size.(Amulya)
%****** Input: Azimuth of collector (phic), tilt of collector (tilt)
%***** Output: [x,y,z] - Coordinates of surface vertices

switch Surface
    case 'Flat Plate'
        ns = 20;
        [X,Y] = meshgrid(  linspace(0,1,ns)  ,  linspace(0,1,ns+1)   );
        Z = (ones(size(X,1),size(X,2)))/2;

        % Adjust Surface for Tilt and Azimuth
        z = -tand(tilt)*X+Z*cosd(tilt);
        x_i = X+Z*sind(tilt);
        x = cosd(phi)*x_i-sind(phi)*Y;
        y = sind(phi)*x_i+cosd(phi)*Y;

    case 'SemiCylinder'
        ns = 20;
        R = ones(ns,1);
        m = length(R);
        theta = (0:ns)/ns*pi;
        X = (((0:m-1)')*ones(1,ns+1))./ max(max(((0:m-
        1)')*ones(1,ns+1)),[],2);
```

```
        Y = ((R*cos(theta))+abs(min(min((R*cos(theta))),[],2)))/...
        (max(max((R*cos(theta))),[],2)+abs(min(min((R*cos(theta))),[],2
        )));
        Z = (R*sin(theta))/2;

        % Adjust Surface for Tilt and Azimuth
        z = -tand(tilt)*X+Z*cosd(tilt);
        x_i = X+Z*sind(tilt);
        x = cosd(phi)*x_i-sind(phi)*Y;
        y = sind(phi)*x_i+cosd(phi)*Y;

    case 'Sinusoidal - pi'
        xsize=1;
        xstep=0.05;
        ysize=1;
        ystep=0.05;
        [X,Y] = meshgrid(0:xstep:xsize,0:ystep:ysize);
        Z =sin(pi*Y);

        z = -tand(tilt)*X+Z*cosd(tilt);
        x_i = X+Z*sind(tilt);
        x = cosd(phi)*x_i-sind(phi)*Y;
        y = sind(phi)*x_i+cosd(phi)*Y;

    case 'Sinusoidal - pi/2'
        xsize=1;
        xstep=0.05;
        ysize=1;
        ystep=0.05;
        [X,Y] = meshgrid(0:xstep:xsize,0:ystep:ysize);
        Z =0.5*sin((pi/2)*Y);

        z = -tand(tilt)*X+Z*cosd(tilt);
        x_i = X+Z*sind(tilt);
        x = cosd(phi)*x_i-sind(phi)*Y;
        y = sind(phi)*x_i+cosd(phi)*Y;

    case 'Sinusoidal - pi/2 - Weighted'
        xsize=1;
        xstep=0.05;
%         ysize=1;
%         ystep=0.05;
%         Yaxis = cat(2,0,logspace(0,2,20)/100)%inverted
        Yaxis = logspace(2,0,20)/100
        Yaxis = cat(2,abs(Yaxis-1),1)
        [X,Y] = meshgrid(0:xstep:xsize,Yaxis);
        Z =1*sin((pi/2)*Y);

        z = -tand(tilt)*X+Z*cosd(tilt);
        x_i = X+Z*sind(tilt);
        x = cosd(phi)*x_i-sind(phi)*Y;
        y = sind(phi)*x_i+cosd(phi)*Y;
```

```
    case 'Ellipsoid'
        ns = 20;
        R = ones(ns,1);
        m = length(R);
        theta = (0:ns)/ns*pi;
            X = (((0:m-1)')*ones(1,ns+1))./ max(max(((0:m-
            1)')*ones(1,ns+1)),[],2);
            Y =((R*cos(theta))
            +abs(min(min((R*cos(theta))),[],2)))/...
            (max(max((R*cos(theta))),[],2) ...
            +abs(min(min((R*cos(theta))),[],2)));
        Z = (R*sin(theta));

        % Adjust Surface for Tilt and Azimuth
        z = -tand(tilt)*X+Z*cosd(tilt);
        x_i = X+Z*sind(tilt);
        x = cosd(phi)*x_i-sind(phi)*Y;
        y = sind(phi)*x_i+cosd(phi)*Y;

    case 'Cone'
        r = 0.5;
        h = 2;
        m = h/r;
        [R,A] = meshgrid(linspace(0.25,r,10),linspace(pi/2,-pi/2,16));
        X = R .* cos(A);
        Y = R .* sin(A);
        Z = m*R;
        % Cone around the z-axis, point at the origin
        % mesh(X,Y,Z)

        phi = pi/2;
        X1 = X*cos(phi) - Z*sin(phi);
        Y1 = Y;
        Z1 = X*sin(phi) + Z*cos(phi);
end
```

Face Function

```
function [Area,Center,Normal,Length,Width,Height] = Face( x,y,z )
%** NOTE: This works only for one degree of freedom from initial point
% Input: [x,y,z]
% Output: [nU,nV,nW] , Normal, Center, Area
%%%%%%%%%%%%%%%%%%%%%%%%%%%%%%%%%%%%%%%%%%%%%%%%%%%%%%%%%%%%%%%%%%%%%%%%%%%
%% Initialize matrices and vertex normals
[U,V,W] = surfnorm(x,y,z);
Vertex = size(x);
    nr = Vertex(1)-1; % Number of Cell Rows
    nc = Vertex(2)-1; % Number of Cell Columns
Center(nr,nc,3) = zeros();
Normal(nr,nc,3) = zeros();
Length = zeros(nc); Width = zeros(nr); Height = zeros(nc);
Area(nr,nc) = zeros();


%% Calculating the normal vector of each face
for idx = 1:1:nr
    for jdx = 1:1:nc
        Normal(idx,jdx,1) = (U(idx,jdx)+U(idx,jdx+1)...
            +U(idx+1,jdx)+U(idx+1,jdx+1))/4;
        Normal(idx,jdx,2) = (V(idx,jdx)+V(idx,jdx+1)...
            +V(idx+1,jdx)+V(idx+1,jdx+1))/4;
        Normal(idx,jdx,3) = (W(idx,jdx)+W(idx,jdx+1)...
            +W(idx+1,jdx)+W(idx+1,jdx+1))/4;
    end;end;

%% Calculating surface center
for idx = 1:1:nr
    for jdx = 1:1:nc
        Center(idx,jdx,1) = (x(idx,jdx)+x(idx,jdx+1)...
            +x(idx+1,jdx)+x(idx+1,jdx+1))/4;
        Center(idx,jdx,2) = (y(idx,jdx)+y(idx,jdx+1)...
            +y(idx+1,jdx)+y(idx+1,jdx+1))/4;
        Center(idx,jdx,3) = (z(idx,jdx)+z(idx,jdx+1)...
            +z(idx+1,jdx)+z(idx+1,jdx+1))/4;
    end:end;

%% Calculating area of face
for idx = 1:1:nr
    for jdx = 1:1:nc
        Length(idx,jdx) = max(abs([x(idx,jdx+1)-x(idx,jdx)...
            ,x(idx+1,jdx)-x(idx,jdx)]));
        Width(idx,jdx)  = max(abs([y(idx,jdx+1)-y(idx,jdx)...
            ,y(idx+1,jdx)-y(idx,jdx)]));
        Height(idx,jdx) = max(abs([z(idx,jdx+1)-z(idx,jdx)...
            ,z(idx+1,jdx)-z(idx,jdx)]));
        Area(idx,jdx) = Length(idx,jdx)*(sqrt(Width(idx,jdx)^2 +...
            Height(idx,jdx)^2));
    end;end;end;
```

Daylight Function

```
function [ Rise,Set ] = Daylight( Lat,Lon,d
%Calculates daylight hours given location and declination angle.
% Output:
%     Rise: hours before Solar Noon (+)
%     Set: Hours after Solar Noon (-
    SHd = acosd(-tand(Lat)*tand(d));
    SHsr = 12 - (SHd/15);
    SHss = 12 + (SHd/15);

    Q = 3.467/(cosd(Lat)*cosd(d)*sind(SHd));

    Sunrise = SHsr - Q/60;
    Sunset = SHss + Q/60;

    Rise = 12 - floor(Sunrise);
    Set = 12 - ceil(Sunset);
end
```

SunFluxPostion

```
sp = zeros(TimeSteps,3);
check = tand(d)/tand(Lat);
kdx = 0;
for j = Rise:StepSize:Set
    kdx = kdx+1;
    H(kdx)=(15*j);
    B(kdx) = max(asind((cosd(Lat)*cosd(d)*cosd(H(kdx)))…
      +(sind(Lat)*sind(d))),0);

    phis(kdx)=asind((cosd(d)*sind(H(kdx)))/cosd(B(kdx)));
    if(cosd(H(kdx))<check && j>0)
        phis(kdx) = 180 - phis(kdx);
    elseif(cosd(H(kdx))<check && j<0)
        phis(kdx) = 180-phis(kdx)-360;
    end
    phisa(kdx)=phis(kdx)+90;

    m(kdx)=1/sind((B(kdx)));    % Air mass ratio
    % Terrestrial Radiation seen on the surface
    tIr(kdx)=A*exp(-(k*m(kdx)));

    az(kdx,1) = phisa(kdx)*pi/180; % Degree to Radian
    el(kdx,1) = B(kdx)*pi/180;    % Degree to Radian
    % Record the sun path
    sp(kdx,1) = sin(az(kdx))*cos(el(kdx));  % u
    sp(kdx,2) = -cos(az(kdx))*cos(el(kdx)); % v
    sp(kdx,3) = sin(el(kdx));             % w
    TOD(kdx) = 12-j;end
```

Insolation Function

```
function [BeamIn, TotalEnergy, EnergyPerHour,Gb,Incidence,
InstaEnergy,VF] = Insolation

evalin('base','save myTEMPvars.mat');
load myTEMPvars.mat

%% *********** Angle between two vectors (Sun and Face)*************
% Initialize matricies
Incidence = zeros(size(Area,1),size(Area,2),numel(Rise:StepSize:Set));
VF = zeros(size(Area,1),size(Area,2),numel(Rise:StepSize:Set));
%  AvgVF = zeros(size(Area,1),size(Area,2),numel(Rise:StepSize:Set));
BeamIn = zeros(size(Area,1),size(Area,2),numel(Rise:StepSize:Set));
%  AvgBeamIn = zeros(TimeSteps,1);
EnergyPerHour = zeros(1,TimeSteps);
%% Begin Iterations

    for kdx = 1:1:TimeSteps
        Sa = sp(kdx,:);
        for idx = 1:size(Area,1)
            for jdx = 1:size(Area,2)
                VecNorm = cat(2,nU(idx,jdx),nV(idx,jdx),nW(idx,jdx));
                Incidence(idx,jdx,kdx) = atan2d ...
                  (norm(cross(VecNorm,Sa)),...
                    dot(VecNorm,Sa));
                if Incidence(idx,jdx,kdx)>90
                    Incidence(idx,jdx,kdx) = 90;
                end;end;end
        % View factors per cell
        VF(:,:,kdx) = cosd(Incidence(:,:,kdx));
        % Average view factor of all cells
            % AvgVF(kdx,:) =  mean2(VF(:,:,kdx));
        % Direct beam insolation per cell
        BeamIn(:,:,kdx) = VF(:,:,kdx).*tIr(kdx);
        % Average direct beam insolation of all cells
        AvgBeamIn(kdx,:) = mean2(BeamIn(:,:,kdx));
        % Total energy per hour
        InstaEnergy = sum(sum(BeamIn(:,:,kdx).*Area),2);
        % Total energy for the day
        EnergyPerHour(kdx) = mean2(InstaEnergy);
    end
    TotalEnergy = sum(EnergyPerHour);
    % Beam Radiation
    Gb = BeamIn/1000;
end
```

Pixelate Function

```
function [PixelRef, PixelMap] = Pixelate(Impp,numPix,TimeSteps)

% Initialize Binning Variable
Tpix = zeros(numel(Impp)/TimeSteps,TimeSteps);
% options = [1.5 100 0.001 0];

    % Compute cluster/group/bin/pixel for each time step
    for kdx = 1:1:TimeSteps
        Tpix(:,kdx) =
            clusterdata(reshape(Impp(:,:,kdx),[],1),'linkage','median',
            numPix);
    end

% Find most prevalent group associated with each cell face
PixelRef = mode(Tpix,2);

PixelMap = reshape(PixelRef , ...
            numel(Impp)/(TimeSteps*length(Impp)), ... % # of Rows
                   length(Impp) % # of Columns
end
```

Pixelate2 Function

```
function [PixelRef1,PixelRef2,PixelRef3] =
Pixelate2(Impp,numPix,TimeSteps)
% Initialize Binning Variable
Tpix = zeros(numel(Impp)/TimeSteps,TimeSteps);
    % Compute cluster/group/bin/pixel for each time step
    for kdx = 1:1:5
        Tpix1(:,kdx) =
clusterdata(reshape(Impp(:,:,kdx),[],1),'linkage','median',numPix);
    end
% Find most prevalent group associated with cell
 PixelRef1 = mode(Tpix1,2);
    for kdx = 6:1:10
        Tpix2(:,kdx) = clusterdata
            (reshape(Impp(:,:,kdx),[],1),'linkage','median',numPix);
    end
% Find most prevalent group associated with cell
PixelRef2 = mode(Tpix2(:,6:10),2);
    for kdx = 11:1:15
        Tpix3(:,kdx) = clusterdata
            (reshape(Impp(:,:,kdx),[],1),'linkage','median',numPix);
    end
    PixelRef3 = mode(Tpix3(:,11:15),2);% Find most prevalent group
end
```

Pixelate3 Function

```
% Find most prevalent group associated with cellfunction [PixelRef,
PixelMap] = Pixelate3(Impp,numPix,TimeSteps)


% Initialize Binning Variable
Tpix = zeros(numel(Impp)/TimeSteps,TimeSteps);
% options = [1.5 100 0.001 0];

    % Compute cluster/group/bin/pixel for each time step
    for kdx = 1:1:TimeSteps

            Tpix(:,kdx) =
clusterdata(reshape(Impp(:,:,kdx),[],1),'linkage','average',numPix);

    PixelMap(:,:,kdx) = reshape(Tpix(:,kdx) , ...
                  numel(Impp)/(TimeSteps*length(Impp)), ... %#rows
                  length(Impp) )              ;             %#Columns
    end
PixelRef = Tpix;
end

%% Find Surface Area
SurfaceArea = sum(sum(Area),2);

%% Find Peak Power
Peak = max(EnergyPerHour);
```